THE UNIVERSITY OF WESTERN ONTARIO
DEPARTMENT OF CIVIL AND
ENVIRONMENTAL ENGINEERING

Water Resources Research Report

Computerized Tool for the Development of Intensity-Duration-Frequency Curves under a Changing Climate

Technical Manual v.1.2

By:
Roshan K. Srivastav
Andre Schardong
and
Slobodan P. Simonovic

Report No: 089
Date: October 2015

ISSN: (print) 1913-3200; (online) 1913-3219;
ISBN: (print) 978-0-7714-3087-9; (online) 978-0-7714-3088-6;

Computerized tool for the Development of Intensity-Duration-Frequency Curves under a Changing Climate

www.idf-cc-uwo.ca

Technical Manual

Version 1.2

October, 2015

By

Roshan K. Srivastav

Andre Schardong

and

Slobodan P. Simonovic

Department of Civil and Environmental Engineering

The University of Western Ontario

London, Ontario, Canada

Executive Summary

Climate change and its effects on nature, humans and the world economy are major research challenges of recent times. Climate observations and numerous studies clearly indicate that climate is changing rapidly under the influence of changing chemical composition of the atmosphere, major modifications of land use and ever-growing population. The increase of concentration of greenhouse gases (GHG) seems to be one of the major driving forces behind climate change.

Global warming has already affected the hydrological and ecological cycle of the earth's system. Among the noticeable modifications of the hydrologic cycle is the change in frequency and intensity of extreme rainfall events, which in many cases result in severe floods. Most of Canada's existing water resources infrastructure has been designed based on the assumption that historical climate is a good predictor of the future. It is now realized that the historic climate will not be representative of future conditions and new and existing water resource systems must be designed or retrofitted to take into consideration changing climate conditions.

Rainfall intensity-duration-frequency (IDF) curves are one of the most important tools for design, operation and maintenance of a variety of water management infrastructures, including sewers, storm water management ponds, street curbs and gutters, catch basins, swales, among a significant variety of other types of infrastructure. Currently, IDF curves are usually developed using historical observed data with the assumption that the same underlying processes will govern future rainfall patterns and resulting IDF curves. This assumption is not valid under changing climatic conditions. Global climate models (GCM) provide understanding of climate change under different future emission scenarios, also known as representative concentration pathways (RCP), and provide a way to update IDF curves under a changing climate. More than 40 GCMs have been developed by various research organizations around the world. However, these GCMs are built to project climate change on large spatial and temporal scales and therefore use of GCMs for modification of IDF curves, which are local or regional in nature, requires some additional steps.

The work presented in this manual is part of the project *"Computerized IDF_CC Tool for the Development of Intensity-Duration-Frequency Curves under a Changing Climate"* supported by Canadian Water Network. The project focuses on (i) the development of a new methodology for updating IDF curves; and (ii) building a web based IDF update tool. This technical manual provides a detailed description of the mathematical models and procedures used within the IDF_CC tool. The accompanied document presents the User's Manual for the IDF_CC tool entitled *"Computerized IDF_CC Tool for the Development of Intensity-Duration-Frequency-Curves under a Changing Climate - User's Manual"* referred further as *UserMan*.

The remainder of the manual is organized as follows. Section 1 introduces the issue of IDF curves under changing climate. In section 2, a brief background review of IDF curves and processes for updating IDF curve information is provided. Section 3 presents the mathematical models that are used for: (i) Fitting probability distributions; (ii) Estimating parameters; (iii) Spatially interpolating GCM data to observed stations; (iv) Selecting GCM models; and (v) Updating IDF curves. Finally, a summary and the conclusions are outlined in section 4.

Contents

List of Figures

List of Tables

1.0 Introduction

Changes in climate conditions observed over the last few decades are considered to be the cause of change in magnitude and frequency of occurrence of extreme events (IPCC 2013). The Fifth Assessment Report (AR5) of the Intergovernmental Panel on Climate Change (IPCC 2013) has indicated a global surface temperature increase of 0.3 to 4.8 °C by the year 2100 compared to the reference period 1986-2005 with more significant changes in tropics and subtropics than in mid-latitudes. It is expected that rising temperature will have a major impact on the magnitude and frequency of extreme precipitation events in some regions (Barnett et al. 2006; Wilcox et al. 2007; Allan et al. 2008; Solaiman et al. 2011). Incorporating these expected changes in planning, design, operations and maintenance of water infrastructure would reduce unseen future uncertainties that may result from increasing frequency and magnitude of extreme rainfall events.

According to the AR5, heavy precipitation events are expected to increase in frequency, intensity, and/or amount of precipitation under changing climate conditions. Table 1 summarizes assessments made regarding heavy precipitation in AR5 (IPCC 2013 – Table SPM.1).

Table 1: Summary of AR5 Assessments for Extreme Precipitation

<table>
<tr><th rowspan="2">Assessment that changes occurred since 1950</th><th rowspan="2">Assessment of a human contribution to observed changes</th><th colspan="2">Likelihood of further changes</th></tr>
<tr><th>Early 21st century</th><th>Late 21st century</th></tr>
<tr><td>Likely more land areas with increases than decreases</td><td>Medium Confidence</td><td rowspan="3">Likely over many land areas</td><td>Very likely over most of the mid-latitude land masses and over wet tropical areas</td></tr>
<tr><td>Likely more land areas with increases than decreases</td><td>Medium confidence</td><td>Likely over many areas</td></tr>
<tr><td>Likely over most land areas</td><td>More likely than not</td><td>Very likely over most land areas</td></tr>
</table>

Since it is evident that the global temperature is increasing with climate change, it follows that the saturation vapor pressure of the air will increase, as this is a function of air temperature. Further, it is observed that the historical precipitation data has shown considerable changes in trends over the last 50 years (Fig. 1 and 2). These changes are likely to intensify with increases in global temperature (IPCC 2013).

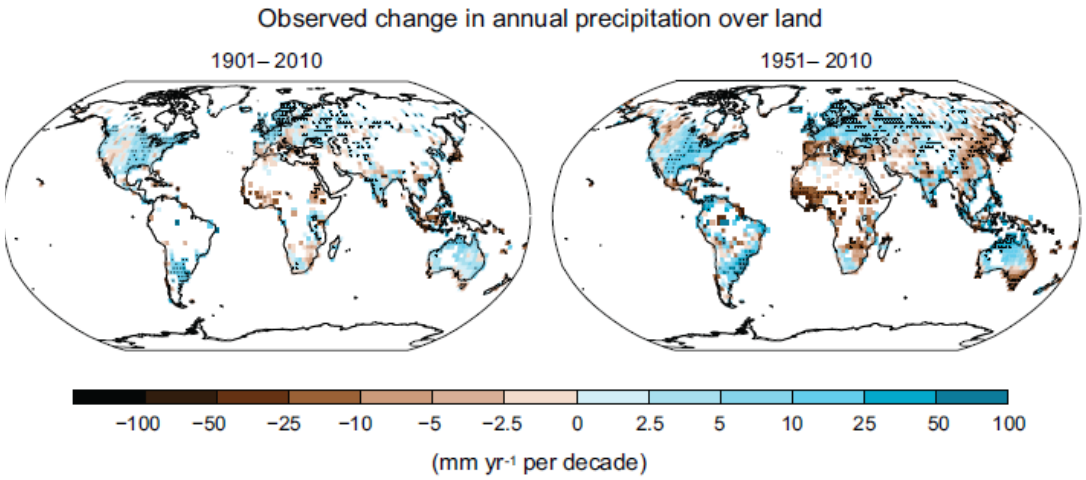

Figure 1: Changes in observed precipitation from 1901 to 2010 and from 1951 to 2010 (after IPCC 2013)

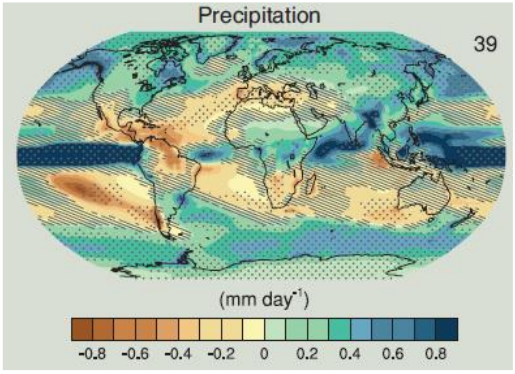

Figure 2: Changes in annual mean precipitation for 2081-2100 relative to 1986-2005 under the Representative Concentration Pathway RCP 8.5. (after IPCC 2013) (see Appendix B)

Evaluation of change in precipitation intensity and frequency is critical as these data are used directly in design and operation of water infrastructure. However, assessment of climate change impacts and the implementation of climate change research is a challenge for many practitioners.

Practitioner application of climate change science remains a challenge for several reasons, including: 1) the complexity of and difficulty in implementing climate change impact assessment methods, which are based on heavy analytical procedures; 2) the academic and scientific communities' focus on publishing research findings under the rigorous peer review processes with limited attention given to practical implementation of findings; 3) political dimensions of climate change issues; and 4) a high level of uncertainty with respect to future climate projections in the presence of multiple climate models and emission scenarios.

This project aimed to develop and implement a generic and simple tool to allow practitioners to easily incorporate impacts of climate change, in form of updated IDF curves, into water infrastructure design and management. To accomplish this task, a web interface based tool has been developed (referred to as the IDF_CC tool), consisting of friendly user interface with a powerful database system and sophisticated, but efficient, methodology for the update of IDF curves.

Intensity duration frequency (IDF) curves are typically developed by fitting a theoretical probability distribution to an annual maximum precipitation (AMP) time series. AMP data is fitted using extreme value distributions like Gumbel, Generalized Extreme Value (GEV), Log Pearson, Log Normal, among other approaches. The IDF curves provide precipitation accumulation depths for various return periods (T) and different durations, usually, 5, 10, 15, 20 30 minutes, 1, 2, 6, 12, 18 and 24 hours. Durations exceeding 24 hours may also be used, depending on the application of IDF curves. Hydrologic design of storm sewers, culverts, detention basins and other elements of storm water management systems is typically performed based on specified design storms derived from the IDF curves (Solaiman and Simonovic, 2010; Peck et al., 2012).

The web based IDF_CC tool is a decision support system (DSS). As such, it includes traditional DSS components including a user interface, database and model base.[1] One of the major components of the IDF_CC decision support system is a model base that includes a set of mathematical models and procedures for updating IDF curves. These mathematical models are

[1] For a detailed description of DSS components, see *UserMan* Section 1.

an important part of the IDF_CC tool and are responsible for the calculations required to develop the IDF curves based on historical data and for updating IDFs to reflect future climatic conditions. The models and procedures used within the IDF_CC tool include:

- Statistical analysis algorithms: statistical analysis is applied to fit the selected theoretical probability distributions to both historical and future precipitation data. To fit the data Gumbel distribution is used in this tool They are fitted using method of moments. The GCM data used in statistical analysis are spatially interpolated from the nearest grid points using the inverse distance method.
- Optimization algorithm: an algorithm used to fit the analytical relationship to an IDF curve.
- GCM Selection algorithm: a quantile regression based algorithm applied to select and/or rank the GCM models according to their skill.[2]
- IDF update algorithm: the equidistant quantile matching – EQM algorithm is applied to the IDF updating procedure.

This technical manual presents the details of the statistical analysis procedures, GCM selection algorithm and IDF update algorithm. For the optimization algorithm, readers are referred to *UserMan* Appendix 1.

[2] The "skill" of a GCM reflects its ability to accurately simulate past or present day climates for a given region.

2.0 Background

2.1 Intensity-Duration-Frequency Curves

Reliable rainfall intensity estimates are necessary for hydrologic analyses, planning, management and design of water infrastructure. Information from IDF curves is used to describe the frequency of extreme rainfall events of various intensities and durations. The rainfall intensity-duration-frequency (IDF) curve is one of the most common tools used in urban drainage engineering, and application of IDF curves for a variety of water management applications has been increasing (CSA, 2010). The guideline for 'Development, Interpretation and Use of Rainfall Intensity-Duration-Frequency (IDF) Information: A Guideline for Canadian Water Resources Practitioners" developed by Canadian Standards Association (CSA, 2012) lists the following reasons for increasing application of rainfall IDF information:

- As the spatial heterogeneity of extreme rainfall patterns becomes better understood and documented, a stronger case is made for the value of "locally relevant" IDF information.
- As urban areas expand, making watersheds generally less permeable to rainfall and runoff, many older water systems fall increasingly into deficit, failing to deliver the services for which they were designed. Understanding the full magnitude of this deficit requires information on the maximum inputs (extreme rainfall events) with which drainage works must contend.
- Climate change will likely result in an increase in the intensity and frequency of extreme precipitation events in most regions in the future. As a result, IDF values will optimally need to be updated more frequently than in the past and climate change scenarios might eventually be drawn upon in order to inform IDF calculations.

The typical development of rainfall IDF curves involves three steps. First, a probability distribution function (PDF) or Cumulative Distribution Function (CDF) is fitted to rainfall data for a number of rainfall durations. Second, the maximum rainfall intensity for each time interval is related with the corresponding return period from the cumulative distribution function. Third, from the known cumulative frequency and given duration, the maximum rainfall intensity can be determined using an appropriate fitted theoretical distribution functions (such as GEV, Gumbel, Pearson Type III, etc.) (Solaiman and Simonovic 2010). The IDF_CC tool adopts Gumbel

distribution for fitting the annual maximum precipitation (AMP). The parameter estimation for the selected distributions is carried out using the method of moments.

2.2 Updating IDF Curves

The main assumption in the process of developing IDF curves is that the historical series are stationary and therefore can be used to represent the future extreme conditions. This assumption is questionable under rapidly changing conditions, and therefore IDF curves that rely only on historical observations will misrepresent future conditions (Sugahara et al. 2009; Milly et al. 2008). Global Climate Modeling (GCM) is one of the best ways to explicitly address changing climate conditions for the future periods (i.e., non-stationary conditions). GCM models simulate atmospheric patterns on larger spatial grid scales (usually greater than 100 kilometers) and hence are unable to represent the regional scale dynamics accurately. In contrast, regional climate models (RCM) are developed to incorporate the local-scale effects and use smaller grid scales (usually 25 to 50 kilometers). The major shortcoming of RCMs is the computational requirements to generate realizations for various atmospheric forcings.

Both GCM and RCM models have larger spatial scales than the size of most watersheds, which is the relevant scale for IDF curves. Downscaling is one of the techniques to link GCM/RCM grid scales and local study areas for the development of IDF curves under changing climate conditions. Downscaling approaches can be broadly classified as either dynamic downscaling or statistical downscaling. The dynamic downscaling procedure is based on limited area models or uses higher resolution GCM/RCM models to simulate local conditions, whereas statistical downscaling procedures are based on transfer functions which relate the GCM models with the local study areas; that is,, a mathematical relationship is developed between the GCM output and historically observed data for the time period of observations. Statistical downscaling procedures are used more widely than dynamic models because of their lower computational requirements and availability of GCM outputs for a wider range of emission scenarios. Table 2 provides comparison between dynamic downscaling and statistical downscaling.

Table 2: Comparison of dynamic downscaling and statistical downscaling

Criteria	Dynamic downscaling	Statistical downscaling
Computational time	Slower	Fast
Experiments	Limited realizations	Multiple realizations
Complexity	More complete physics	Succinct physics
Examples	Regional climate models, Nested GCMs	Linear regression, Neural network, Kernel regression

The IDF_CC tool adopts an equidistant quantile-matching (EQM) method for updating IDF curves, developed by Srivastav et al. (2014), which can capture the distribution of changes between the projected time period and the baseline period (temporal downscaling) in addition to spatial downscaling the annual maximum precipitation (AMP) derived from the GCM data and the observed sub-daily data. In the case of the EQM method, the quantile-mapping functions are directly applied to annual maximum precipitation (AMP) to establish the statistical relationships between the AMPs of GCM and sub-daily observed (historical) data rather than using complete daily precipitation records. This methodology is relatively simple (in terms of modelling complexities) and computationally efficient. Figure 3 explains a simplified approach to update for EQM method used in IDF_CC tool to update IDF curves. The three main steps which are involved in using EQM method are: (i) establish statistical relationship between the AMPs of the GCM and the observed station of interest, which is referred as spatial downscaling (See Figure 3 dark brown arrow); and (ii) establish statistical relationship between the AMPs of the base period GCM and the future period GCM, which is which is referred as temporal downscaling (See Figure 3 black arrow); and (iii) establish statistical relationship between steps (i) and (ii) to update the IDF curves for future periods (See Figure 3 red arrow).

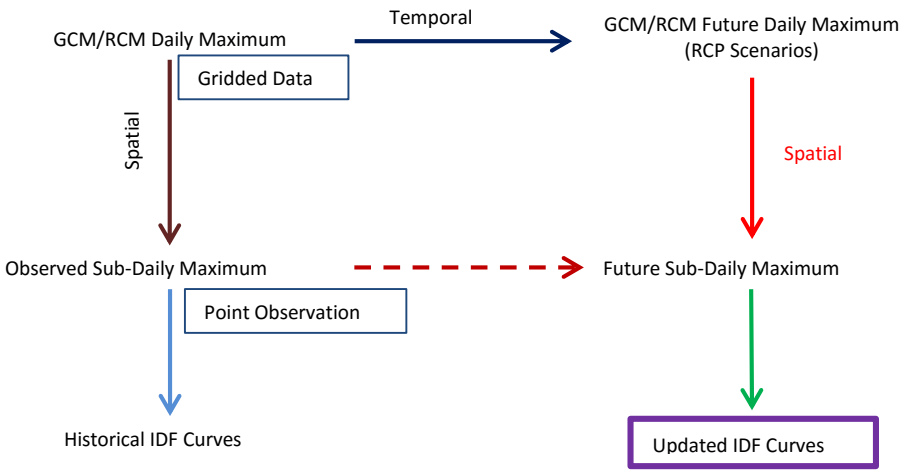

Figure 3: Concept of Equidistance quantile matching method for updating IDF curves

2.3 Global Climate Models (GCM) and Representative Concentration Pathways

General Climate Models (GCM) represent the dynamics within the Earth's atmosphere to understand current and future climatic conditions. These models are the best tools for assessment of the impacts of climate change. There are numerous GCMs developed by different climate research centres. They are all based on (i) land-ocean-atmosphere coupling; (ii) greenhouse gas emissions, and; (iii) different initial conditions representing the state of the climate system. These models simulate global climate variables on coarse spatial grid scales (e.g., 250 km by 250 km) and are expected to mimic the dynamics of regional-scale climate conditions. The GCMs are extended to predict the atmospheric variables under the influence of climate change due to global warming. The amount of greenhouse gas emissions is the key variable for generating future scenarios. Other factors that may influence the future climate include land-use, energy production, global and regional economy and population growth.

To update the IDF curves under changing climatic conditions, the IDF_CC tool uses 22 GCMs from different climate research centers (see *UserMan:* Section 3.2). The GCM outputs are usually available in the netCDF format that is widely used for storing climate data. The IDF_CC tool converts the netCDF files into a more efficient format in order to reduce storage space and computational time. These converted climate data files are stored in the IDF_CC tool's database (see *UserMan:* Section 1.2). The salient features of each of the GCMs used in the IDF_CC tool is presented in Appendix B. The data for the various GCMs can be downloaded from

https://www.earthsystemgrid.org/home.htm which is a gateway for scientific data collections. These models are adopted based on the availability of complete sets of future greenhouse gas concentration scenarios, also known as Representative Concentration Pathways (RCPs) described in detail in the IPCC AR5 report (See: IPCC Fifth Assessment Report – Annex 1 Table: AI.1), and briefly described below.

Based on the initial conditions that represent the state of the climate system, GCMs generate different time series that are known as 'Runs'. Multiple Runs are conducted to help account for uncertainty related to initial conditions. Updating IDF curves using all the time series that include Runs from each of the GCMs would be computationally demanding. Therefore the IDF_CC tool provides three options (*UserMan:* Section 3.2), including: (i) select a GCM based on skill score or (ii) select any model from the list of GCMs provided in the tool or (iii) select ensemble. The selection of GCM based on skill scores will rank the models in the order of their skill. That is, the first model listed for the user will have the highest skill score, followed subsequently by each model ranked in order of their declining skill scores. This method automatically allows the user to select the best GCM for updating the IDF curves. The user can choose the second option to test any of the GCM models to update the IDF curves. The users are encouraged to test different models due to the uncertainty associated with climate modeling (*UserMan:* Section 3.2).

The Fifth Assessment Report (AR5) of the Intergovernmental Panel on Climate Change (IPCC) introduced new future climate scenarios associated with Representative Concentration Pathways (RCPs), which are based on time-dependent projections of atmospheric greenhouse gas (GHG) concentrations. RCPs are scenarios that include time series of emissions and concentrations of the full suite of greenhouse gases, aerosols and chemically active gases, as well as land use and land cover factors (Moss et al., 2008). The word "representative" signifies that each RCP provides only one of many possible scenarios that would lead to the specific radiative forcing[3]

[3] Radiative forcing is the change in the net, downward minus upward, radiative flux (expressed in Wm^{-2}) at the tropopause or top of atmosphere due to a change in external driver of climate change, such as, for example, a change in the concentration of carbon dioxide or the output of the sun (IPCC AR5, annex III)

characteristics. The term "pathway" emphasizes that not only the long-term concentration levels are of interest, but also the trajectory taken over time to reach that outcome (Moss et al. 2010).

There are four RCP scenarios: RCP 2.6, RCP 4.5, RCP 6.5 and RCP 8.5. The following definitions are adopted directly from IPCC AR5 (IPCC 2013):

RCP2.6: One pathway where radiative forcing peaks at approximately 3 W m^{-2} before 2100 and then declines (the corresponding Extended Concentration Pathways[4] (ECP) assuming constant emissions after 2100).

RCP4.5 and RCP6.0: Two intermediate stabilization pathways in which radiative forcing is stabilized at approximately 4.5 W m^{-2} and 6.0 W m^{-2} after 2100 (the corresponding ECPs assuming constant concentrations after 2150).

RCP8.5: One high pathway for which radiative forcing reaches greater than 8.5 W m^{-2} by 2100 and continues to rise for some time (the corresponding ECP assuming constant emissions after 2100 and constant concentrations after 2250).

The future emission scenarios used in the IDF_CC tool are based on RCP2.6, RCP4.5 and RCP8.5 (*UserMan:* Section 3.2 and 3.3). RCP2.6 represents the lower bound, followed by RCP4.5 as an intermediate level and RCP 8.5 as the higher bound. IDF curves developed using RCP2.6 and RCP8.5 represent the range of uncertainty or possible range of IDF curves under changing climatic conditions. Similar to GCMs, the future emission scenarios for each GCM (i.e., the RCPs) have different Runs based on the initial conditions imposed on the model. The number of updated IDF curves from a particular RCP scenario will be equal to the number of runs available for a selected GCM. The IDF_CC tool has two representations of future IDF curves (*UserMan:* Section 3.3): (i) updated IDF curve for each RCP scenario where the IDF curves are averaged from all the GCMs and their scenarios and (ii) comparison of future and historical IDF curves.

[4] Extended concentration pathways describes extensions of the RCP's from 2100 to 2500 (IPCC AR5, annex III)

2.4 Selection of GCM models

According to the fifth assessment report of IPCC, there are 42 GCM models developed by various research centres (Refer: Table AI.1 from Annex I IPCC AR5). In IDF_CC tool, adopts only 22 GCM models out of the 42 listed GCMs because: i) Not all the GCMs generate the three selected RCPs for future climate scenarios (i.e., RCP 2.6, 4.5 and 8.5); and ii) there are some technical issues related to downloading (such as connection to remote servers or repositories) for some GCM models. Currently, the IDF_CC tool uses all 22 GCMs that have all the three future climate scenarios available for updating the IDF curves (*UserMan:* Section 3.2). However, the use of all the 22 GCMs in the IDF_CC tool could be computationally demanding. In order to reduce uncertainty due to choice of the GCMs, the tool applies a skill score algorithm to rank the GCMs provided in the tool. The IDF_CC tool adopts a skill score based on quantile regression (QRSS) proposed by Srivastav et al. (2015) (Appendix E) to assess the performance of different GCM models available for use within the tool. The QRSS approach has two main components: (i) the quantiles representing the distribution of the data; (ii) the quantile regression lines representing the trends and heteroscedasticity across the quantiles. The QRSS has the ability to capture (i) the distributional characteristics; and (ii) the error statistics. In order to avoid the risks of claiming a false precision in our ability to distinguish credible from non-credible scenarios, which could lead to bad decisions by end users IPCC typically includes most or all members of CMIP multi-model ensembles in their uncertainty analysis. The IDF_CC tool provides an option to the user to generate the ensemble of all the 22 GCMs.

2.5 Historical Data

In the case of historical data sets, the IDF_CC tool has a repository of Environment Canada stations. However, the user can provide their own dataset and develop future IDF curves. For more detail on how to use user-defined historical datasets, refer to *UserMan:* Section 2.6. The historical datasets used in the IDF_CC tool for development of future IDF curves has to satisfy the following conditions:

1. **Data length:** The minimum length of the historical data to calculate the IDF curves should be equal to or greater than 10 years.
2. **Missing Values:** The IDF_CC tool does not infill and/or extrapolate missing data. The user should provide complete data without missing values.

3.0 Mathematical Models and Procedures used by IDF_CC

The mathematical models of the IDF_CC tool and are responsible for calculations required to develop the IDFs based on the historical data and IDFs updated for future climate. The models and procedures used within the IDF_CC tool include: (i) statistical analysis for fitting Gumbel distribution using method of moments and inverse distance method for spatial interpolation (*UserMan:* section 3.1); (ii) GCM selection algorithm (*UserMan:* section 3.2 and 3.3); and (iii) IDF updating algorithm (*UserMan:* section 3.2 and 3.3). In this section the algorithms and their implementation within the IDF_CC tool are presented.

The implementation of each algorithm is illustrated using a simple example. The examples use historical observed data from Environment Canada for a London, Ontario station and GCM data for the base period and future time period from the Canadian global climate model CanESM2, spatially interpolated to the London station. The data are presented in Appendix C. For simplicity the examples use 24hr annual maximum precipitation. The same procedure can be followed for other durations.

3.1 Statistical Analysis

3.1.1 Probability Distribution Function

The Gumbel distribution is adopted for use by the IDF_CC tool. It has a wide variety of applications for estimating extreme values of given data sets, and is commonly used in hydrologic applications. It is used to generate the extreme precipitations at higher return periods for different durations (*UserMan:* section 3.2 and 3.3). The statistical distribution analysis is a part of the mathematical models used in the decision support system of the IDF_CC tool (*UserMan:* sections 1.4). The following sections explain the theoretical details of the statistical analyses implemented within the tool.

3.1.1.1 Gumbel Distribution (EV1)

The EV1 distribution has been widely recommended and adopted as the standard distribution by Environment Canada for all the Precipitation Frequency Analyses in Canada. The EV1 distribution for annual extremes can be expressed as:

$$Q_t = \mu + K_T \sigma \quad (1)$$

where Q_t is the exceedance value, μ and σ are the population mean and standard deviation of the annual extremes; T is return period in years

$$K_T = -\frac{\sqrt{6}}{\pi}\left[0.5772 + \ln\left(\ln\left(\frac{T}{T-1}\right)\right)\right] \quad (2)$$

3.1.2 Parameter Estimation

A common statistical procedure for estimating distribution parameters is the use of a maximum likelihood estimator or the method of moments. Environment Canada uses and recommends the use of the method of moments technique to estimate the parameters for EV1. The IDF_CC tool uses the method of moments to calculate the parameters of the Gumbel distribution (*UserMan:* Section 1.4 and 3.1). The following describes the method of moments procedure for calculating the parameters of the Gumbel distribution.

3.1.2.1 Method of Moments

The most popular method for estimating the parameters of the Gumbel distribution is method of moments (Hogg et al., 1989). In case of Gumbel distribution, the number of unknown parameters is equal to the mean and standard deviation of the sample mean. The first two moments of the sample data will be sufficient to derive the parameters of the Gumbel distribution in Eq: 1. These are defined as:

$$\mu = \frac{1}{N}\sum_{i=1}^{N} Q_i \quad (3)$$

$$\sigma = \sqrt{\frac{1}{N-1}\sum_{i=1}^{N}\left(Q_i - \bar{Q}\right)^2} \quad (4)$$

Example: 3.1

The step-by-step procedure followed in IDF_CC tool (*UserMan:* Section 3.1) for the estimation of the Gumbel distribution (EV1) parameters are.

1. Calculate the mean of the historical data using Eq. 3

$$\mu = \frac{1}{N}\sum_{i=1}^{N} Q_i = 53.67$$

2. Calculate the value of standard deviation of the historical data using Eq. 4

$$\sigma = \sqrt{\frac{1}{N-1}\sum_{i=1}^{N}\left(Q_i - \bar{Q}\right)^2} = 17.46$$

3. Calculate the value of K_T for a given return period (assuming return period (T) equal to 100years) using Eq 2

$$K_T = -\frac{\sqrt{6}}{\pi}\left[0.5772 + \ln\left(\ln\left(\frac{T}{T-1}\right)\right)\right] = -\frac{\sqrt{6}}{\pi}\left[0.5772 + \ln\left(\ln\left(\frac{100}{100-1}\right)\right)\right] = 3.14$$

4. Calculate the precipitation for a given return period using Eq 1.

$$Q_t = \mu + K_T\sigma = 53.67 + 3.14 \times 17.46 = 108.43$$

5. Finally the precipitation intensities are calculated for different return periods and frequencies. The IDF curves using the Gumbel distribution for the historical data is obtained as

	Return Period T					
Duration	**2**	**5**	**10**	**25**	**50**	**100**
5 min	9.15	12.00	13.88	16.26	18.03	19.78
10 min	13.29	18.14	21.35	25.41	28.42	31.41
15 min	16.00	21.74	25.53	30.33	33.89	37.42
30 min	20.60	28.22	33.26	39.63	44.36	49.05
1 h	24.51	35.15	42.19	51.09	57.69	64.24
2 h	29.54	41.21	48.94	58.70	65.94	73.13
6 h	36.67	47.89	55.32	64.71	71.68	78.59
12 h	42.89	54.05	61.43	70.76	77.68	84.55
24 h	50.80	66.23	76.44	89.35	98.92	108.43

3.1.3 Spatial Interpolation of GCM data

As discussed above, GCM spatial grid size scales are too coarse for application in updating IDF curves, and usually range above $1.5^o \times 1.5^o$ [5]. To capture the distribution changes between the projected time period and the baseline period (downscaling) the GCM data has to be spatially interpolated for the station coordinates. In the IDF_CC tool an inverse square distance weighting method, in which the nearest four grid points to the station are weighted by an inverse distance function from the station to the grid points, is applied (*UserMan*: Section 3.2). In this way the grid points that are closer to the station are weighted more than the grid points further away from the station. The mathematical expression for the inverse square distance weighting method is given as:

$$w_i = \frac{1/d_i^2}{\sum_{i=1}^{k} 1/d_i^2} \qquad (5)$$

where d_i is the distance between the i^{th} GCM grid point and the station, k is the number of nearest grid points - equal to 4 in the IDF_CC tool.

Example: 3.2

A hypothetical example shows calculation of spatial interpolation using inverse distance method. In this example the historical observation station lies within four grid points. The procedure followed in the IDF_CC tool for the inverse distance method is as follows:

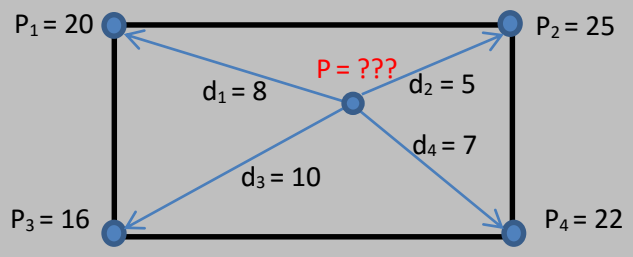

[5] Conversion from degrees to length (distance in km)

degrees	N/S or E/W at equator	E/W at 23N/S	E/W at 45N/S	E/W at 67N/S
1.0	111.32 km	102.47 km	78.71 km	43.496 km

1. Calculate the weights using inverse distance method using equation 5:

$$w_1 = \frac{1/d_i^2}{\sum_{i=1}^{k} 1/d_i^2} = \frac{\frac{1}{8^2}}{\frac{1}{8^2}+\frac{1}{5^2}+\frac{1}{10^2}+\frac{1}{7^2}} = 0.167286$$

$$w_2 = \frac{1/d_i^2}{\sum_{i=1}^{k} 1/d_i^2} = \frac{\frac{1}{5^2}}{\frac{1}{8^2}+\frac{1}{5^2}+\frac{1}{10^2}+\frac{1}{7^2}} = 0.428253$$

$$w_3 = \frac{1/d_i^2}{\sum_{i=1}^{k} 1/d_i^2} = \frac{\frac{1}{10^2}}{\frac{1}{8^2}+\frac{1}{5^2}+\frac{1}{10^2}+\frac{1}{7^2}} = 0.107063$$

$$w_4 = \frac{1/d_i^2}{\sum_{i=1}^{k} 1/d_i^2} = \frac{\frac{1}{7^2}}{\frac{1}{8^2}+\frac{1}{5^2}+\frac{1}{10^2}+\frac{1}{7^2}} = 0.297398$$

2. Calculate the spatially interpolated precipitation using the above weights

$$\begin{aligned} P &= P_1 w_1 + P_2 w_2 + P_3 w_3 + P_4 w_4 \\ &= 20 \times 0.167286 + 25 \times 0.428253 + 16 \times 0.107063 + 22 \times 0.297398 \\ &= 22.30781 \end{aligned}$$

3.2 Selection of GCM Using Quantile Regression

The IDF_CC tool uses a quantile regression based skill score (QRSS) algorithm developed by Srivastav and Simonovic (2014) for the selection and/or ranking of GCM (*UserMan*: Section 3.2 and 3.3). First a brief description of quantile regression and its mathematical formulation is presented. Next, the methodology for using QRSS for ranking the GCM models is presented. The mathematical expression of quantile regression is presented below (after Koenker and Bassett, 1978).

Let the precipitation be represented by X and denoted by:

$$X = \{x_1, x_2, ..., x_t\} \quad (6)$$

where t is index for time and can be denoted by:

$$t = \{1, 2, 3, \cdots, T\} \tag{7}$$

For a given α^{th} quantile the linear model is expressed as:

$$x_i = t_i' \beta_\alpha + e_i \quad i = 1, ..., T \tag{8}$$

where x is precipitation; t' is transpose of variable time; α is the quantile; T is the length of total time period; and e is the residual error.

Let $Q_\alpha(X|t)$ represents the relationship between the precipitation and time in eq (8) and can be expressed as:

$$Q_\alpha(X|t) = t'\beta_\alpha \tag{9}$$

The parameter β_α at αth quantile can be written as:

$$\hat{\beta}_\alpha = \arg\min_{\beta} \sum_{i=1}^{n} f_\alpha(x_i - t_i'\beta) \tag{10}$$

where the function $f_\alpha(u)$ for any value u is given as:

$$f_\alpha(u) = \begin{cases} u(\alpha - 1) \ \ if\ u < 0 \\ u(\alpha) \ \ if\ u \geq 0 \end{cases} \tag{11}$$

The estimate of the regression quantile can be expressed as:

$$\hat{Q}_\alpha(X|t) = t'\hat{\beta}_\alpha \tag{12}$$

The function for $\hat{\beta}_\alpha$ is monotonic and hence would result in an optimal solution. The parameter $\hat{\beta}_\alpha$ can be solved using linear programming. More details on the quantile regression can be found in Koenker (2005) and Srivastav and Simonovic (2014) (see Appendix E). The following section describes the use of quantile regression in obtaining the GCM skills.

3.2.1 Quantile Regression Based Skill Score Method (QRSS)

Srivastav et al. (2014) developed quantile regression based skill score method (QRSS), in which the quantiles cover the distribution of the data and the coefficients of the linear quantile function

to capture the biases (distance or error) between the GCM output and historical observed data. The steps involved in calculation of QRSS are as follows:

Let the historical observed precipitation data X^H, the GCM model data X^G and the quantiles *A* be represented as:

$$X^H = \left\{x_1^H, x_2^H, ..., x_t^H\right\} \tag{13}$$

$$X^G = \left\{x_1^G, x_2^G, ..., x_t^G\right\} \tag{14}$$

$$\mathrm{A} = \left\{\alpha_1, \alpha_2, ..., \alpha_n\right\} \tag{15}$$

where the superscript H and G represent historical and GCM model data, respectively; and n is the number of quantiles considered.

For a given quantile level α, the linear quantile function is given as:

$$\hat{X}^{H,\alpha} = a^{\alpha,H}t + b^{\alpha,H} \quad \forall t = 1,2,3,\ldots,T \tag{16}$$

$$\hat{X}^{G,\alpha} = a^{\alpha,G}t + b^{\alpha,G} \quad \forall t = 1,2,3,\ldots,T \tag{17}$$

where *a* and *b* represent the coefficients of linear quantile function as slope and intercept, respectively at α^{th} quantile; *t* is the time variable; and *T* is the total time period.

It is expected that the GCM models should be able to generate the variable values close to the historical observed data. However, the models are not perfect and exhibit systematic bias and variability in the generation process. The degree of bias between the GCM model data set and the observed data set is calculated as:

$$S_{bias} = \sum_{i=1}^{k} \sqrt{\frac{1}{T}\sum_{i=1}^{T}\left[\hat{X}_i^{\mathrm{H},\alpha_i} - \hat{X}^{G,\alpha_i}\right]^2} \tag{18}$$

where k is the total number of quantiles used in the study.

The above equation is simply the root mean square error between the quantile lines of observed and GCM data. The bias at various quantile levels (representing the distributional characteristics of the data) is estimated by using equation 18. In order to address the issue of difference in trends, in this study we propose to use a penalty function, which would assign a penalty to equation 18 whenever the trends are different from the historical observed trends. The similarity of the slopes of quantile lines are calculated using a Student's t-test. The following steps compare the two slopes:

1. To statistically test two slopes are equal, the null hypothesis H_o^a and the alternate hypothesis H_1^a, for a given quantile a is defined as

$$H_o^a : a^{a,H} = a^{a,G} \quad i.e., \; a^{a,H} - a^{a,G} = 0 \tag{19}$$

$$H_1^a : a^{a,H} \neq a^{a,G} \quad i.e., \; a^{a,H} - a^{a,G} \neq 0 \tag{20}$$

2. Assuming that the difference between the two slopes has normal distribution, the test statistics is given as

$$t^a = \frac{a^{a,H} - a^{a,G}}{s_{a^{a,H} - a^{a,G}}} \text{ with } (n_1+n_2-4) \text{ degrees of freedom} \tag{21}$$

where $s_{a^{a,H} - a^{a,G}}$ is the standard error of estimated slopes; n_1 and n_2 is the length of the observed and GCM observed data

3. The standard error of the slopes is calculated as

$$s_{a^{a,H} - a^{a,G}} = \sqrt{s^2_{a^{a,H}} + s^2_{a^{a,H}}} = s_{res}\sqrt{\frac{1}{s_H^2(n_1 - 1)} + \frac{1}{s_G^2(n_2 - 1)}} \tag{22}$$

where s_{res} is the pooled residual variance, which is equal to

$$s_{res} = \frac{(n_1 - 2)s^2_{res,H} + (n_2 - 2)s^2_{res,GCM}}{(n_1 - 2) + (n_2 - 2)} \tag{23}$$

4. If the value of t in equation is greater than the Student's t-distribution, the null hypothesis is accepted, i.e., the slopes of the observed data and the GCM data for a given quantile are equal. The t-statistics for the given quantile line is simplified as

$$t^a = \begin{cases} 0 & \textit{if null hypothesis is accepted} \\ 1 & \textit{otherwise} \end{cases} \tag{24}$$

The effect of the dissimilarity of slopes between the observed data and the GCM data is obtained by multiplying a penalty factor to the overall bias. Equation 18 can be rewritten as

$$SS = S_{bias} \times \xi \tag{25}$$

where ξ is the penalty factor based on t-test and is obtained as

$$\xi = 1 + \frac{1}{k}\sum_{i=1}^{k} t^{\alpha_i} \tag{26}$$

where k is the total number of quantiles lines used in the study.

The skill scores obtained in the equation 20 are normalized using inter-quantile range of the observed distribution, which could provide interpretation of scores in terms of the overall spread of the distribution of observations. The quantile regression based skill scores is given as

$$S_{QR} = \frac{SS}{IQ_H} \tag{27}$$

where IQ_H is the inter-quantile range of the historical observations.

The best GCMs should have the S_{QR} values close to zero.

3.3 Updating IDF curves under a Changing Climate

The updating procedure for IDF curves is a part of the mathematical models used in the decision support system of the IDF_CC tool (*UserMan:* section 1.4). The tool uses an equidistant quantile matching (EQM) method to update the IDF curves under changing climate conditions (*UserMan:* section 3.0). The two main steps of the EQM method are: (i) spatial downscaling of the maximum precipitation values from the daily global climate models (GCM) data to each of the sub-daily maximums observed at a station of interest using quantile-mapping functions; and (ii) temporal downscaling to explicitly capture the changes in the GCM data between the baseline period and the future period using quantile-mapping function. The flow chart for the EQM methodology is shown in Fig 4.

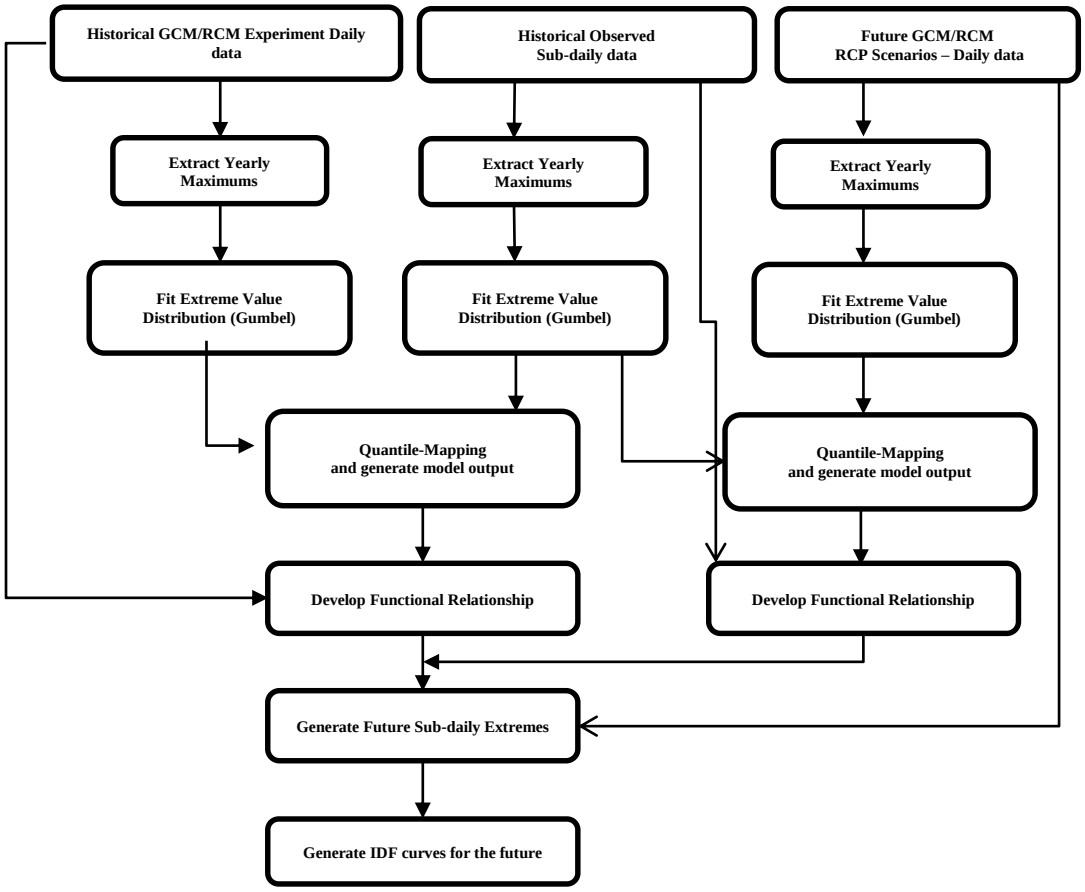

Figure 4: Equidistance Quantile-Matching Method for generating future IDF curves under Climate Change

3.3.1 Equidistance Quantile Matching Method

The following section presents the EQM method for updating the IDF curves using IDF_CC tool. The steps involved in the algorithm are as follows:

(i) Extract sub-daily maximums from the observed data at a given location (i.e., maximums of 5min, 10min, 15min, 1hr, 2hr, 6hr, 12hr, 24hr precipitation data) (*UserMan*: Section 3.1):

$$X_{\max}^{STN} = \begin{bmatrix} X_{1,\max}^{STN,5\min} & X_{1,\max}^{STN,10\min} & \cdots & X_{1,\max}^{STN,24hr} \\ X_{2,\max}^{STN,5\min} & X_{2,\max}^{STN,10\min} & \cdots & X_{2,\max}^{STN,24hr} \\ X_{3,\max}^{STN,5\min} & X_{3,\max}^{STN,10\min} & \cdots & X_{3,\max}^{STN,24hr} \\ \vdots & \vdots & \vdots & \vdots \\ X_{N,\max}^{STN,5\min} & X_{N,\max}^{STN,10\min} & \cdots & X_{N,\max}^{STN,24hr} \end{bmatrix} \quad (28)$$

where $X_{i,\max}^{STN,j}$ represents the maximum sub-daily precipitation at a station (STN) for jth duration in ith year; and N is the total number of years.

(ii) Extract daily (24hr) maximums for the historical base period from the selected GCM model (*UserMan*: Section 3.2)

$$X_{\max}^{GCM} = \begin{bmatrix} X_{1,\max}^{GCM} \\ X_{2,\max}^{GCM} \\ X_{3,\max}^{GCM} \\ \vdots \\ X_{N,\max}^{GCM} \end{bmatrix} \tag{29}$$

where $X_{i,\max}^{GCM}$ represents the maximum daily precipitation from GCM model in ith year and N is the total number of years (same time span from the historical observed data is used).

(iii) Extract daily maximums from the RCP Scenarios (i.e., RCP26, RCP45, RCP85) for the selected GCM model (*UserMan*: Section 3.2):

$$X_{\max}^{GCM,Fut} = \begin{bmatrix} X_{1,\max}^{GCM,RCP26} & X_{1,\max}^{GCM,RCP45} & X_{1,\max}^{GCM,RCP85} \\ X_{2,\max}^{GCM,RCP26} & X_{2,\max}^{GCM,RCP45} & X_{2,\max}^{GCM,RCP85} \\ X_{3,\max}^{GCM,RCP26} & X_{3,\max}^{GCM,RCP45} & X_{3,\max}^{GCM,RCP85} \\ \vdots & \vdots & \vdots \\ X_{N_F,\max}^{GCM,RCP26} & X_{N_F,\max}^{GCM,RCP45} & X_{N_F,\max}^{GCM,RCP85} \end{bmatrix} \tag{30}$$

where $X_{\max}^{GCM,Fut}$ represents the maximum daily precipitation for the future scenarios considered; and N_F is the total number of years considered for future time period.

(iv) Fit a probability distribution to the daily maximums from GCM model (each of the sub-daily maximum series for the observed data and daily maximums for the future scenarios) (*UserMan*: Section 3.2):

$$PDF^{GCM} = f\left(\theta^{GCM} / X_{\max}^{GCM}\right) \tag{31}$$

$$PDF_j^{STN} = f\left(\theta^{STN,j} / X_{\max}^{STN,j}\right) \tag{32}$$

$$PDF^{GCM,Fut} = f\left(\theta^{GCM} / X_{\max}^{GCM,Fut}\right) \quad (33)$$

where PDF stands for probability distribution function, f() is the function, θ is the parameter of the fitted distribution

(v) The cumulative probability distribution of the GCM and the sub-daily series are equated to establish a statistical relationship between them and obtain GCM modeled sub-daily series $Y_{\max,j}^{GCM}$ using the principle of quantile based mapping. This is *spatial downscaling* of the data from the GCM daily maximums to observed sub-daily maximums (*UserMan*: Section 3.2):

$$Y_{\max,j}^{STN} = invCDF\left(\left(CDF\left(X_{\max}^{GCM} / \theta^{GCM}\right)\right) / \theta^{STN,j}\right) \quad (34)$$

where $Y_{\max,j}^{STN}$ is statistically downscaled sub-daily maximum series for j[th] duration; CDF stands for cumulative probability distribution function; and invCDF stands for inverse CDF.

(vi) Establish a similar quantile-mapping statistical relationship which models the change between the current GCM maximums and future GCM maximums. This is *temporal downscaling* of the data from the projected GCM simulations of daily maximums to baseline GCM daily maximums (*UserMan*: Section 3.2):

$$Y_{\max}^{GCM,Fut} = invCDF\left(\left(CDF\left(X_{\max}^{GCM} / \theta^{GCM}\right)\right) / \theta^{GCM,Fut}\right) \quad (35)$$

where $Y_{\max}^{GCM,Fut}$ is quantile matching between the baseline period and the projection period.

(vii) Find an appropriate function to relate $Y_{\max,j}^{STN}$ and $X_{\max}^{GCM}$. Piani et al. (2010) suggested that in most cases the relation is observed to be linear. It is evident from the Gumbel CDF (eq. 3) that it results in a linear equation when equating the two CDFs. It is important to note that there is no guarantee that the use of other distribution functions would result in the similar linear first order equations (*UserMan*: Section 3.2).

$$Y_{\max,j}^{STN} = f\left(X_{\max}^{GCM}\right) \quad (36)$$

$$Y_{\max,j}^{STN} = a_1 \times X_{\max}^{GCM} + b_1 \quad (37)$$

(viii) Find an appropriate function to relate $Y_{\max}^{GCM,Fut}$ and $X_{\max}^{GCM}$ (*UserMan*: Section 3.2):

$$Y_{\max}^{GCM,\text{Fut}} = f\left(X_{\max}^{GCM}\right) \tag{38}$$

$$Y_{\max}^{GCM,Fut} = a_2 \times X_{\max}^{GCM} + b_2 \tag{39}$$

(ix) To generate future maximum sub-daily data, combine equations (37) and (38) by replacing $X_{\max}^{GCM}$ to $Y_{\max}^{GCM,Fut}$ in equation (39) (*UserMan*: Section 3.2):

$$X_{\max,j}^{STN,future} = a_1 \times \left[\frac{X_{\max}^{GCM,future} - b_2}{a_2}\right] + b_1 \tag{40}$$

(x) Generate IDF curves for the future sub-daily data and compare the same with the historically observed IDF curves to obtain the change in intensities.

A MATLAB code for updating the IDF curves using the equidistance quantile matching algorithm is presented in Appendix A.

EXAMPLE: 3.6

The step-by-step procedure followed by the IDF_CC tool for updating IDF curves (*UserMan*: Section 3.2 and 3.3):

1. To update the IDF curves use three sets of datasets: (i) daily (24hr) maximums $X_{\max}^{GCM}$ for the base period from the selected GCM model; (ii) sub-daily maximums from the observed data at a given location (i.e., maximums of 5min, 10min, 15min, 1hr, 2hr, 6hr, 12hr, 24hr precipitation data); and (iii) daily maximums from the RCP Scenarios (i.e., RCP26, RCP45, RCP85) for the selected GCM model. For the case example all the three data sets are in Appendix C
2. Develop a relationship between the sub-daily historical observed and GCM base period as well as between the GCM based period and GCM future time period maximum precipitation data by fitting a probability distribution (see example 3.1)

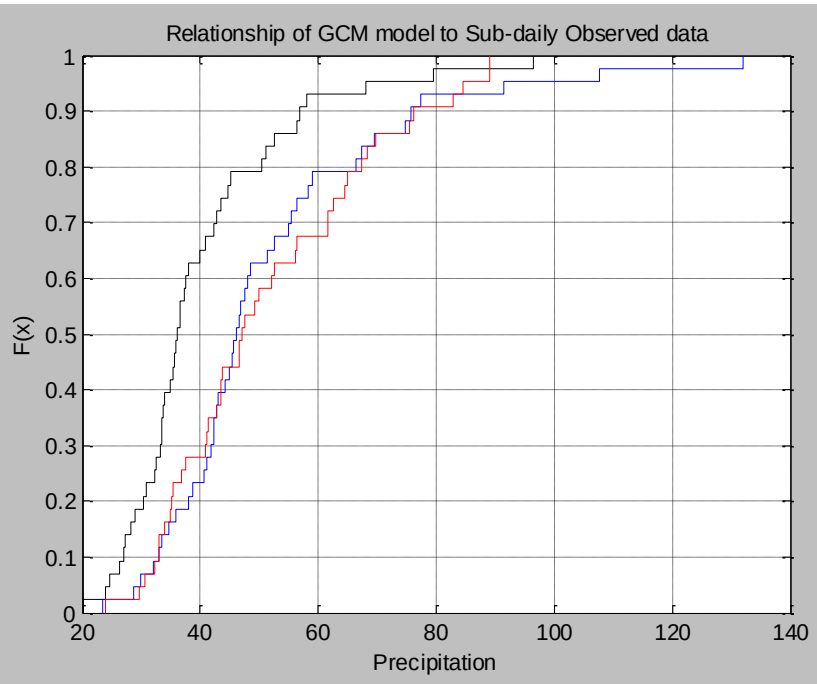

Empirical cumulative probability distribution showing the model output (solid blue line) by statistically relating the maximums of GCM model (solid black line) to the sub-daily observed maximum data (solid red line).

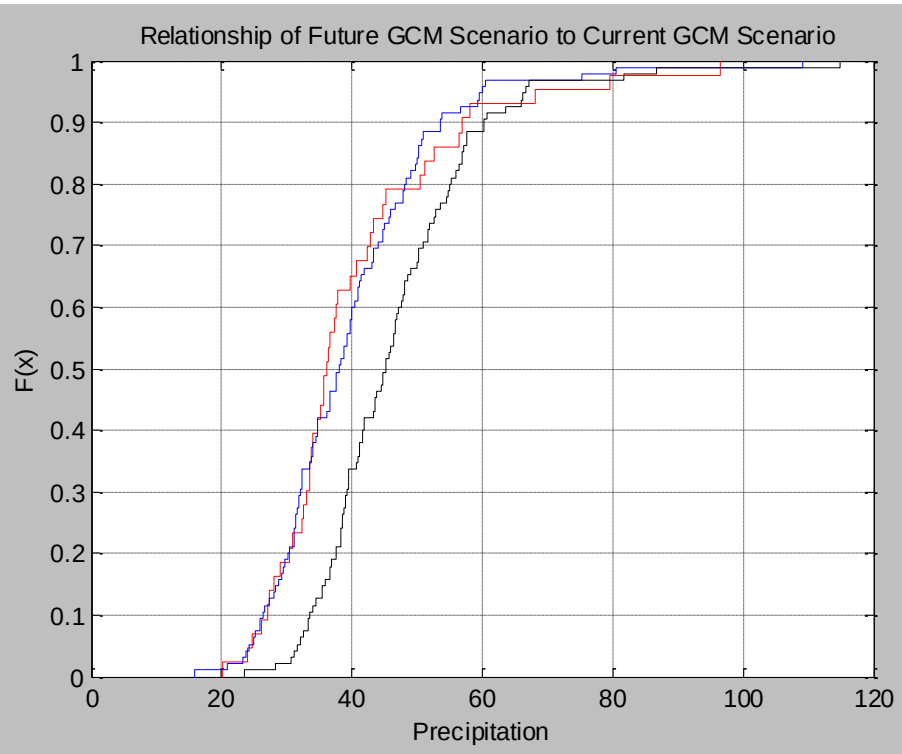

Empirical cumulative probability distribution showing the model output (solid blue line) by statistically relating the maximums of RCP future data (solid black line) to the maximums of the current period GCM data (solid red line).

3. Using equation 34 spatially downscale the data from the GCM daily maximums to observed sub-daily maximums as shown below.

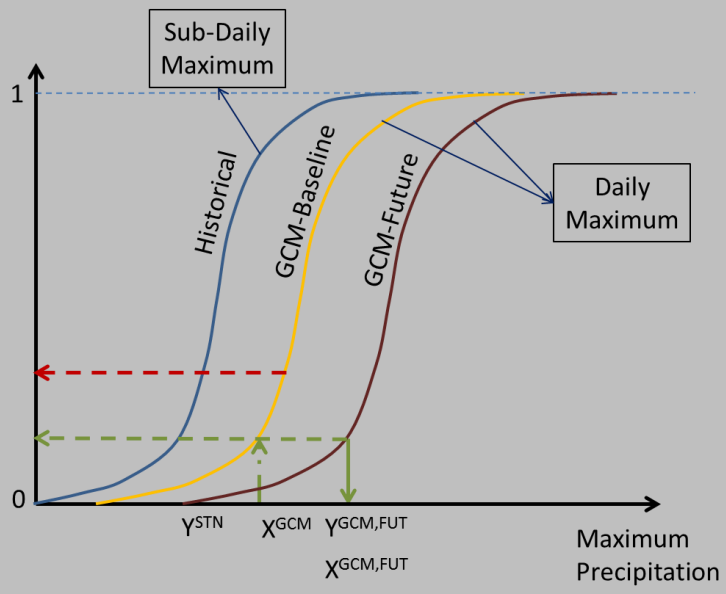

4. Using equation 35 establish the temporal downscaling of the data from the projected GCM simulations of daily maximum to baseline GCM daily maximums.

5. Fit a linear first order equation to relate $Y_{\max,j}^{STN}$ and $X_{\max}^{GCM}$ in equations 37.

$$Y_{\max,j}^{STN} = a_1 \times X_{\max}^{GCM} + b_1 = 1.756391 \times X_{\max}^{GCM} - 17.5867$$

6. Similarly, find an appropriate function to relate $Y_{\max}^{GCM,Fut}$ and $X_{\max}^{GCM}$ in equations 39.

$$Y_{\max}^{GCM,Fut} = a_2 \times X_{\max}^{GCM} + b_2 = 0.995552 \times X_{\max}^{GCM} + 0.077941$$

7. Combine steps 5 and 6 to obtain the future generated data at London station as

$$X_{\max,j}^{STN,future} = a_1 \times \left[\frac{X_{\max}^{GCM,future} - b_2}{a_2} \right] + b_1 = 1.756391 \times \left[\frac{X_{\max}^{GCM,future} - 0.077941}{0.995552} \right] - 17.5867$$

8. Generate IDF curves for the future sub-daily data

London							
	Scenario				***Change in % to historical***		
Minutes	***Historical***	***RCP-26***	***RCP-45***	***RCP-85***	***RCP-26***	***RCP-45***	***RCP-85***
5	109.5	129.0	135.6	155.8	17.80%	23.86%	42.30%
10	79.2	94.5	99.7	115.6	19.34%	25.93%	45.97%
15	63.6	75.8	79.9	92.5	19.12%	25.63%	45.45%
30	41.1	49.4	52.2	60.9	20.28%	27.19%	48.21%
60	24.5	30.1	31.9	37.7	22.70%	30.43%	53.96%
120	14.8	18.1	19.2	22.7	22.57%	30.25%	53.65%
360	6.1	7.2	7.5	8.6	17.36%	23.27%	41.26%
720	3.6	4.2	4.4	5.0	16.28%	21.83%	38.70%
1440	2.1	2.5	2.7	3.1	19.64%	26.34%	46.70%

4. Summary and Conclusion

This document presents the technical reference manual for the *Computerized IDF_CC tool for the Development of Intensity-Duration-Frequency-Curves Under a Changing Climate*. The tool uses a sophisticated although very efficient methodology that incorporates changes in the distributional characteristics of GCM models between the baseline period and the future period. The mathematical models and procedures used within the IDF_CC tool include: (i) Statistical analysis algorithm, which includes fitting Gumbel probability distribution function using method of moments and spatial interpolation of GCM data using inverse distance method; (ii) GCM selection using quantile regression skill score; and (iii) IDF updating algorithm based on equidistance quantile matching method. The document also presents the step-by-step guide for the implementation of all the mathematical models and procedures.

The IDF_CC tool's website (www.idf-cc-uwo.com) should be regularly visited for the latest updates of the IDF_CC tool, new functionalities and updated documentation.

References

Allan RP, Soden BJ (2008) Atmospheric warming and the amplification of precipitation extremes. Science 321*:* 1480–1484.

Barnett DN, Brown SJ, Murphy JM, Sexton DMH, Webb MJ (2006) Quantifying uncertainty in changes in extreme event frequency in response to doubled CO_2 using a large ensemble of GCM simulations. Climate Dynamics 26*(*5*):* 489–511, *DOI: 10.1007/S00382-005-0097-1*.

CSA (Canadian Standards Association). (2012). TECHNICAL GUIDE: Development, interpretation, and use of rainfall intensity-duration-frequency (IDF) information: Guideline for Canadian water resources practitioners. Mississauga: Canadian Standards Association.

Hassanzadeh E, Nazemi A, Elshorbagy, A. (2013) Quantile-Based Downscaling of Precipitation using Genetic Programming: Application to IDF Curves in the City of Saskatoon. *J. Hydrol. Eng.*, 10.1061/(ASCE)HE.1943-5584.0000854

Hog WD, Carr DA, Routledge B (1989) Rainfall Intensity-Duration-Frequency values for Canadian locations. Downsview; Ontario; Environment Canada; Atmospheric Environment Service.

Kao SC, Ganguly AR (2011). Intensity, duration, and frequency of precipitation extremes under 21st-century warming scenarios. Journal of Geophysical Research, 116(D16), D16119. doi:10.1029/2010JD015529

Kharin VV, Zwiers FW, Zhang X, Hegerl G (2007) Changes in temperature and precipitation extremes in the IPCC ensemble of global coupled model simulations. J Climate 20: 1519-1444

Li H, Sheffield J, Wood EF (2010) Bias correction of monthly precipitation and temperature fields from Intergovernmental Panel on Climate Change AR4 models using equidistant quantile matching. *Journal of Geophysical Research*, *115*(D10), D10101. doi:10.1029/2009JD012882

Mailhot A, Duchesne S, Caya D, Talbot G (2007). Assessment of future change in intensity-duration-frequency (IDF) curves for Southern Quebec using the Canadian Regional Climate Model (CRCM). Journal of Hydrology, 347: 197–210. doi:10.1016/j.jhydrol.2007.09.019

MATLAB version 7.12.0. Natick, Massachusetts: The MathWorks Inc., April 8, 2011.

Milly PCD, Julio Betancourt, Malin Falkenmark, Robert M Hirsch, Zbigniew W Kundzewicz, Dennis P Lettenmaier, Ronald J Stouffer (2008) Stationarity Is Dead: Whither Water Management?, *Science, 319 (5863), 573-574. [DOI:10.1126/science.1151915]*

Mirhosseini G, Srivastava P, Stefanova L (2012). The impact of climate change on rainfall Intensity–Duration–Frequency (IDF) curves in Alabama. Regional Environmental Change, *13*(S1), 25–33. doi:10.1007/s10113-012-0375-5

Millington N, Samiran D, Simonovic SP (2011). The comparison of GEV, Log-Pearson Type-3 and Gumbel Distribution in the Upper Thames River Watershed under Global Climate Models. Water Resources Research Report no. 077, Facility for Intelligent Decision Support, Department of Civil and Environmental Engineering, London, Ontario, Canada, 54 pages. ISSN: (print) 1931-3200; (online) 1919-3219.

Nguyen VTV, Nguyen TD, Cung A (2007) A statistical approach to downscaling of sub-daily extreme rainfall processes for climate-related impact studies in urban areas. *Water Science & Technology: Water Supply*, *7*(2), 183. doi:10.2166/ws.2007.053

Peck A, Prodanovic P, Simonovic SP. (2012). Rainfall Intensity Duration Frequency Curves Under Climate Change: City of London, Ontario, Canada. Canadian Water Resources Journal, 37(3), 177–189. doi:10.4296/cwrj2011-935

Piani C, Weedon GP, Best M, Gomes SM, Viterbo P, Hagemann S, Haerter JO. (2010). Statistical bias correction of global simulated daily precipitation and temperature for the application of hydrological models. Journal of Hydrology, 395(3-4), 199–215. doi:10.1016/j.jhydrol.2010.10.024

Simonovic SP, Vucetic D (2012) Updated IDF curves for London, Hamilton, Moncton, Fredericton and Winnipeg for use with MRAT Project, Report prepared for the Insurance Bureau of Canada, Institute for Catastrophic Loss Reduction, Toronto, Canada, 94 pages.

Simonovic SP, Vucetic D (2013) Updated IDF curves for Bathurst, Coquitlam, St, John's and Halifax for use with MRAT Project, Report prepared for the Insurance Bureau of Canada, Institute for Catastrophic Loss Reduction, Toronto, Canada, 54 pages.

Solaiman TA, Simonovic SP (2011) Development of Probability Based Intensity-Duration-Frequency Curves under Climate Change. Water Resources Research Report no. 072, Facility for Intelligent Decision Support, Department of Civil and Environmental Engineering, London, Ontario, Canada, 89 pages. ISBN: (print) 978-0-7714-2893-7; (online) 978-0-7714-2900-2.

Solaiman TA, Simonovic SP (2010) National centers for environmental prediction -national center for atmospheric research (NCEP-NCAR) reanalyses data for hydrologic modelling on a basin scale (2010) *Canadian Journal of Civil Engineering*, 37 (4), pp. 611-623.

Solaiman TA, King LM, Simonovic SP (2011) Extreme precipitation vulnerability in the Upper Thames River basin: uncertainty in climate model projections. Int. J. Climatol., 31: 2350–2364. doi: 10.1002/joc.2244

Srivastav RK, Andre Schardong, Slobodan P. Simonovic (2014), Equidistance Quantile Matching Method for Updating IDF Curves under Climate Change, Water Resources Management, doi: 10.1007/s11269-014-0626-y

Srivastav RK, Slobodan P. Simonovic (2014), Quantile Regression for Selection of GCMs, Climate Dynamics (under review)

Sugahara Shigetoshi, Rocha RP, Silveira R (2009) Non-stationary frequency analysis of extreme daily rainfall in Sao Paulo , Brazil, 29, 1339–1349. doi:10.1002/joc.

Taylor KE, Stouffer RJ, Meehl GA (2012) An overview of CMIP5 and the experiment design. Bull Am Met Soc 93(4):485–498. doi:10.1175/bams-d-11-00094.1

Walsh J (2011) Statistical Downscaling, NOAA Climate Services Meeting, 2011.

Wilby RL, Dawson CW (2007) SDSM 4.2 – A decision support tool for the assessment of regional climate change impacts. Version 4.2 User Manual.

Wilcox EM, Donner LJ (2007) The frequency of extreme rain events in satellite rain-rate estimates and an atmospheric general circulation model. Journal of Climate 20*(*1*):* 53–69.

Acknowledgements

The authors would like to acknowledge the financial support by the Canadian Water Network Project under Evolving Opportunities for Knowledge Application Grant to the third author and Dan Sandink from ICLR - Institute for Catastrophic Loss Reduction for his support and assistance with this project.

Appendix – A: MATLAB code to update IDF curves

UPDATE IDF CURVES – MATLAB CODE

Contents

Intensity-Duration-Frequency Curves Under Climate Change

```
% Author: Roshan K. Srivastav

% Method: Equidistance Quantile Matching

% Citation: Roshan K. Srivastav, Andre Schardong, Slobodon P. Simonovic,
%         Equidistance Quantile Matching Method for Updating IDF Curves under Climate
%         Change, Water Resources Management, 2014
%         Doi: 10.1007/s11269-014-0626-y
```

Clear Workspace and Command Window

```
clear all
close all
clc
```

Input Data

```
% Load Input Data
% Includes: Sub-daily Maximums, GCM base period daily maximum, GCM future
%         period daily maximum

load input_data

% Sub-daily Time Interval
subdaily = [5,10,15,30,60,120,360,720,1440];
% Return Period
RT = [2,5,10,25,50,100];
P = 1./RT;
```

FIT Extreme value distribution

```
% Fitting Gumbel Distribution
% Negative sign for Gumbel distribution
% Positive is for minimums for evfit
IDF = zeros(size(data_hist,2),length(P));
hist_error = zeros(size(data_hist,2),length(P));
```

```
future_change1 = zeros(size(data_hist,2),length(P));
future_change2 = zeros(size(data_hist,2),length(P));
IDF_gen = zeros(size(data_hist,2),length(P));
IDF_gen1 = zeros(size(data_hist,2),length(P));
IDF_gen2 = zeros(size(data_hist,2),length(P));
IDF_gen3 = zeros(size(data_hist,2),length(P));

mtrA = zeros(size(data_hist,2), 4);
mtrPar = zeros(size(data_hist,2), 6);

for i = 1:size(data_hist,2)

   max_hist_con = data_hist(:,i);

   % Fitting Gumbel Distribution
   parm_maxfit_hist = evfit(-max_hist_con);
   parm_maxfit_gcm = evfit(-max_gcm_con);
   parm_maxfit_gcm_fut = evfit(-max_gcm_fut);


   mtrPar(i,1) = -parm_maxfit_hist(1); mtrPar(i,2) = parm_maxfit_hist(2);
   mtrPar(i,3) = -parm_maxfit_gcm(1); mtrPar(i,4) = parm_maxfit_gcm(2);
   mtrPar(i,5) = -parm_maxfit_gcm_fut(1); mtrPar(i,6) = parm_maxfit_gcm_fut(2);


   pre_model = evinv(evcdf(-max_gcm_con,parm_maxfit_gcm(1,1),parm_maxfit_gcm(1,2)),...
      parm_maxfit_hist(1,1),parm_maxfit_hist(1,2));

   pre_model_fut = evinv(evcdf(-
max_gcm_fut,parm_maxfit_gcm_fut(1,1),parm_maxfit_gcm_fut(1,2)),...
      parm_maxfit_gcm(1,1),parm_maxfit_gcm(1,2));

   pre_model_fut_reverse = evinv(evcdf(-
max_gcm_con,parm_maxfit_gcm(1,1),parm_maxfit_gcm(1,2)),...
      parm_maxfit_gcm_fut(1,1),parm_maxfit_gcm_fut(1,2));

   post_para = polyfit(max_gcm_con,-pre_model,1);
   post_para3 = polyfit(-pre_model_fut_reverse,max_gcm_con,1);

   pre_model1 = polyval(post_para,max_gcm_con);

   % Not accommodating Future Change
   pre_model_fut1 = polyval(post_para,max_gcm_fut);

   % Accommodating Future Change
   a1 = post_para(1,1);b1 =post_para(1,2);
```

```
    a2 = post_para3(1,1);b2 = post_para3(1,2);
    pre_model_fut3 = (a1*((max_gcm_fut-b2)./a2))+b1;

    %Historical IDF
    IDF(i,:) = -(evinv(P,parm_maxfit_hist(1,1),parm_maxfit_hist(1,2)))*(60/subdaily(i));

    parm_maxfit_gcm0 = evfit(-pre_model1);
    parm_maxfit_gcm3 = evfit(-pre_model_fut3);

    % GCM IDF for Historical Time Period
    IDF_gen(i,:) = -(evinv(P,parm_maxfit_gcm0(1,1),parm_maxfit_gcm0(1,2)))*(60/subdaily(i));

    % GCM IDF for Equidistant Quantile Mapping Future Time Period
    IDF_gen3(i,:) = -
(evinv(P,parm_maxfit_gcm3(1,1),parm_maxfit_gcm3(1,2)))*(60/subdaily(i));

end

% Plot to generate Cumulative Probability Distribution Function
figure
h1= cdfplot(max_gcm_con);
set(h1, 'Color','black')
hold on
h2 = cdfplot(-pre_model);
set(h2, 'Color','blue')
h3 = cdfplot(max_hist_con);
set(h3,'Color','red')
xlabel('Precipitation');

% Plot to generate Cumulative Probability Distribution Function
figure
plot(IDF_gen3','o-')
set(gca,'XTickLabel',{'2';'5';'10';'25';'50';'100'});
title('Updated IDF Curve');
xlabel('Return Period');
ylabel('Intensities');
legend('Duration','Location','NorthWest')
```

Graphical Outputs:

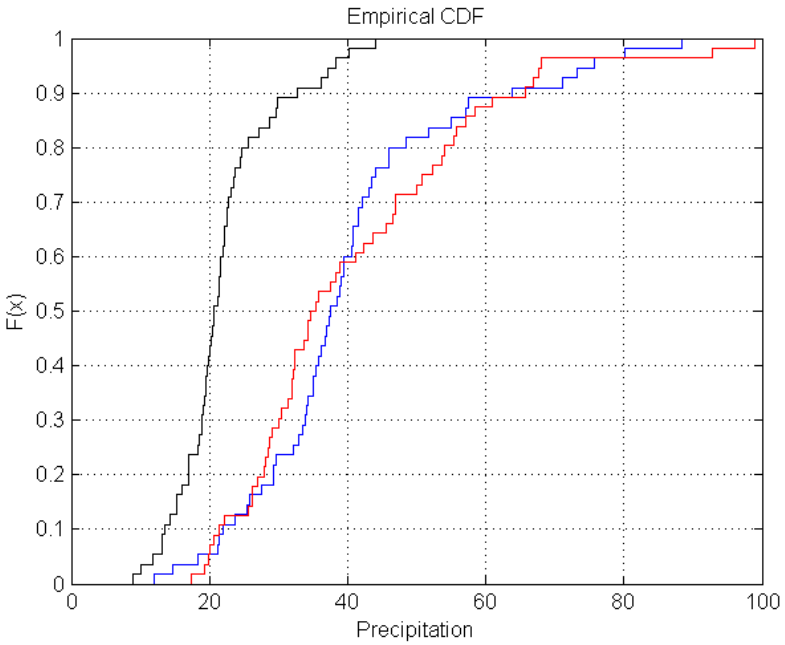

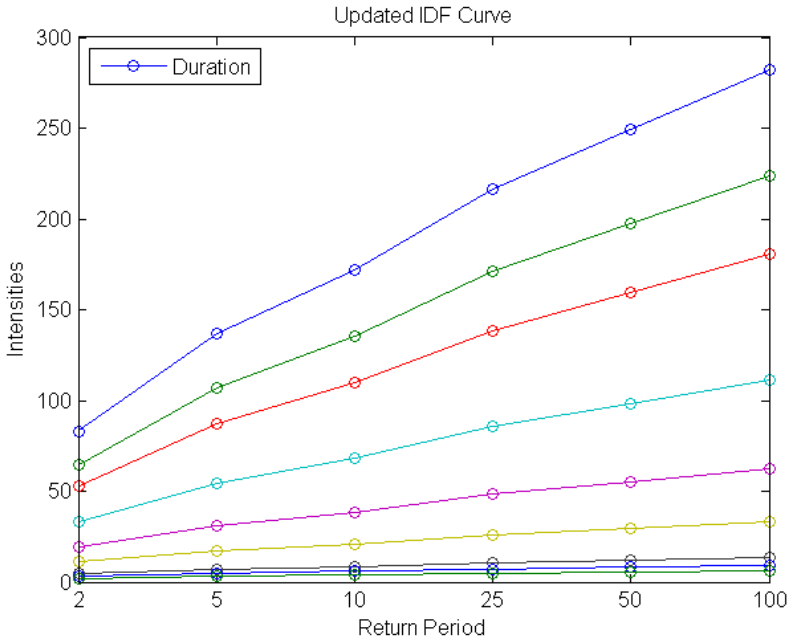

Appendix – B: GCMs used in IDF_CC tool

The selected CMIP5 models and their attributes which has all the three emission scenarios (RCP2.6, RCP4.5 and RCP8.0)

Country	Centre Acronym	Model	Centre Name	Number of Ensembles (PPT)	GCM Resolutions (Lon. vs Lat.)
China	BCC	bcc_csm1_1	Beijing Climate Center, China Meteorological Administration	1	2.8 x 2.8
China	BCC	bcc_csm1_1 m	Beijing Climate Center, China Meteorological Administration	1	
China	BNU	BNU-ESM	College of Global Change and Earth System Science	1	2.8 x 2.8
Canada	CCCma	CanESM2	Canadian Centre for Climate Modeling and Analysis	5	2.8 x 2.8
USA	CCSM	CCSM4	National Center of Atmospheric Research	1	1.25 x 0.94
France	CNRM	CNRM-CM5	Centre National de Recherches Meteorologiques and Centre Europeen de Recherches et de Formation Avancee en Calcul Scientifique	1	1.4 x 1.4
Australia	CSIRO3.6	CSIRO-Mk3-6-0	Australian Commonwealth Scientific and Industrial Research Organization in collaboration with the Queensland Climate Change Centre of Excellence	10	1.8 x 1.8
USA	CESM	CESM1-CAM5	National Center of Atmospheric Research	1	1.25 x 0.94
China	LASG-CESS	FGOALS_g2	IAP (Institute of Atmospheric Physics, Chinese Academy of Sciences, Beijing, China) and THU (Tsinghua University)	1	2.55 x 2.48
USA	NOAA GFDL	GFDL-CM3	National Oceanic and Atmospheric Administration's Geophysical Fluid Dynamic Laboratory	1	2.5 x 2.0
USA	NOAA GFDL	GFDL-ESM2G	National Oceanic and Atmospheric Administration's Geophysical Fluid Dynamic Laboratory	1	2.5 x 2.0
United Kingdom	MOHC	HadGEM2-AO	Met Office Hadley Centre	1	1.25 x 1.875
United Kingdom	MOHC	HadGEM2-ES	Met Office Hadley Centre	2	1.25 x 1.875
France	IPSL	IPSL-CM5A-LR	Institut Pierre Simon Laplace	4	3.75 x 1.8
France	IPSL	IPSL-CM5A-MR	Institut Pierre Simon Laplace	4	3.75 x 1.8
Japan	MIROC	MIROC5	Japan Agency for Marine-Earth Science and Technology	3	1.4 x 1.41
Japan	MIROC	MIROC-ESM	Japan Agency for Marine-Earth Science and Technology	1	2.8 x 2.8

Country	Centre Acronym	Model	Centre Name	Number of Ensembles (PPT)	GCM Resolutions (Lon. vs Lat.)
Japan	MIROC	MIROC-ESM-CHEM	Japan Agency for Marine-Earth Science and Technology	1	2.8 x 2.8
Germany	MPI-M	MPI-ESM-LR	Max Planck Institute for Meteorology	3	1.88 x 1.87
Germany	MPI-M	MPI-ESM-MR	Max Planck Institute for Meteorology	3	1.88 x 1.87
Japan	MRI	MRI-CGCM3	Meteorological Research Institute	1	1.1 x 1.1
Norway	NOR	NorESM1-M	Norwegian Climate Center	3	2.5 x 1.9

Appendix – C: Case Example: Station London

The following is the observed annual maximum precipitation for station London obtained from Environment Canada, which includes for the duration of 5min, 10min, 15min, 30min, 1hr, 2hr, 6hr, 12hr and 24hr.

Year	t5min	t10min	t15min	t30min	t1h	t2h	t6h	t12h	t24h
1943	18.3	24.1	26.2	36.3	51.1	53.8	53.8	56.1	78.7
1944	7.6	8.1	11.2	15.2	21.1	34.3	47	51.8	56.1
1945	6.6	9.7	12.7	17.3	19.3	25.4	34.3	39.4	47.8
1946	13.2	14.5	15.5	29.7	48.3	60.5	61.5	61.5	83.3
1947	10.9	19.3	23.9	29.2	29.2	29.2	40.9	43.2	46.7
1952	7.9	12.7	15.2	28.7	30.5	30.5	38.4	39.9	74.2
1953	15.7	24.6	36.8	56.9	83.3	83.3	83.3	83.3	83.3
1954	10.9	12.7	17	21.6	29.2	32.8	39.1	52.6	78
1955	6.6	9.1	11.2	14.2	14.7	17.3	32.5	44.2	51.1
1956	9.1	10.7	11.7	16.8	20.1	35.3	40.4	42.7	53.8
1957	6.3	9.4	12.4	16.5	26.2	28.2	35.6	47.5	55.6
1958	7.6	9.7	11.2	15.7	16.5	18.5	29.2	39.1	39.9
1959	8.6	10.9	13	15.5	23.4	39.6	50.3	50.5	50.5
1960	9.1	12.7	16.8	27.7	28.2	38.9	39.9	42.4	46.7
1961	11.4	20.1	23.9	29	39.9	43.2	43.4	43.4	43.4
1962	8.6	16.5	17	17	18.8	26.7	29	34.8	35.1
1963	5.6	7.9	9.1	10.4	10.4	11.4	21.3	21.3	23.9
1964	7.9	10.9	14.2	19	23.9	32.3	38.1	59.2	67.3
1965	5.6	10.4	11.7	14.2	18.3	21.1	29	38.4	43.7
1966	8.4	8.4	8.9	14.2	19.3	27.4	43.9	52.6	52.6
1967	7.9	11.9	12.2	19.3	20.6	22.4	33.5	37.3	41.4
1968	10.4	13.2	16	24.6	28.7	32.3	53.1	67.6	84.6
1969	6.9	10.2	13.5	15.7	15.7	18.5	27.4	39.9	47.5
1970	10.9	13	16.5	17	21.1	22.1	23.9	33.3	36.8
1971	8.9	15	22.4	32.5	39.1	42.7	42.7	42.7	42.7
1972	14.5	20.1	22.9	22.9	34.3	40.6	58.4	59.7	62.5
1973	7.4	9.4	13.5	17	17.8	19.6	31.5	40.4	52.1
1974	4.8	7.9	9.1	10.9	13.2	22.4	29.2	30.2	35.3
1975	9.1	12.4	15.2	18.5	21.1	21.1	27.9	30.5	30.5
1976	18.5	26.9	27.7	29.2	30.5	30.7	37.8	40.9	50
1978	6.6	10.9	14.2	14.4	14.4	14.4	23.5	27.3	29.6
1979	19.2	33.5	37.6	45.9	46	46	46.6	65.4	68.2
1980	11.5	20.6	27.8	30.6	32.5	32.6	37.7	47.1	61.7
1981	10.1	12.5	13.2	13.2	16.2	26.7	35	37.5	43.5
1982	6.8	10.8	15.1	22.2	24.6	28.6	35.4	36.8	37.6

1983	13.5	23.4	29.5	37.6	41.1	41.1	47	55.8	64.4
1984	9.8	10.6	14.5	27.4	27.8	43.5	50.8	56	69.7
1985	8.3	10.9	13.7	22.8	29	35.1	43.2	56.8	65
1986	12.4	22.7	24.2	24.5	30.6	42.2	43.8	49.7	89.1
1987	6.7	9.4	11	13.2	14.3	17.7	27.2	44.5	56.5
1988	7.9	11.2	15.5	18.2	18.3	26.9	33	41.9	61.6
1989	8.7	10.9	13.5	23.3	25.7	25.8	25.8	34	34.8
1990	11.9	16.7	18.7	30.4	35.1	37.9	41.6	54.1	75.5
1991	9.7	11.6	13.9	17.5	20.6	22	28.1	32.2	32.2
1992	6.5	11.5	15.9	20.9	35	45.2	51.8	58.6	76.3
1993	9.4	14.3	15.1	19.1	21.9	25	28.5	30.7	49.2
1994	7.5	11.3	12.1	16.8	20.6	33.2	38.9	40.3	46.5
1995	8.2	11.3	12.6	15.8	21.8	28	37.8	45	56.1
1996	9.4	15.8	17.9	26.1	39.2	68.1	82.7	83.5	89
1997	10.6	17	19.6	21.8	21.8	24.8	31.1	33.9	33.9
1998	12.6	14.7	15.8	17.6	20.4	20.4	20.4	-99.9	33
1999	7.3	11.2	11.8	12.7	13.3	19	25.9	26.1	32.9
2000	11.5	15.3	17.6	23	30.6	40.6	-99.9	-99.9	82.8
2001	6.3	7.9	10.6	13.2	13.4	14	24	35	41.2
2003	10	18.4	23.2	26.2	26.2	27.8	31.2	40.8	40.8
2004	15	23.6	27.2	29.4	29.4	29.6	45.4	47	47
2005	9	12.6	15.4	19.8	19.8	24	35.6	37	45.6

The spatially interpolated GCM data for the base period at station London is provided in the following table

Year	Base Period
1943	34.63
1944	34.43
1945	34.28
1946	51.60
1947	32.92
1948	50.02
1949	37.82
1950	32.21
1951	42.36
1952	43.10
1953	38.08
1954	28.46
1955	35.80
1956	26.83
1957	33.12

1958	44.76
1959	37.43
1960	54.24
1961	38.72
1962	27.76
1963	27.76
1964	34.52
1965	40.38
1966	34.68
1967	33.76
1968	34.89
1969	45.03
1970	41.13
1971	46.69
1972	35.53
1973	59.03
1974	31.32
1975	29.93
1976	49.26
1977	35.04
1978	44.41
1979	21.62
1980	20.91
1981	31.51
1982	46.85
1983	50.55
1984	41.23
1985	46.08
1986	34.22
1987	42.09
1988	27.97
1989	39.61
1990	54.70
1991	40.46
1992	42.18
1993	54.02
1994	45.39
1995	42.75
1996	35.68
1997	43.81
1998	69.71
1999	39.77
2000	55.65

2001	48.19
2002	65.94
2003	37.12
2004	59.16
2005	36.84

The spatially interpolated future emission scenarios (RCP) data at station London is provided in the following table

Year	RCP 2.6	RCP 4.5	RCP 8.5
2006	45.1622	57.745	31.74
2007	48.53682	31.256	53.89
2008	36.85236	40.106	28.71
2009	41.17063	36.583	49.78
2010	40.93406	40.890	49.84
2011	55.58957	42.050	42.66
2012	39.65082	50.934	20.78
2013	29.20486	43.575	30.35
2014	37.10033	43.321	40.98
2015	70.95828	32.892	34.43
2016	33.26686	39.338	46.30
2017	36.90782	39.642	49.66
2018	41.95582	42.081	48.48
2019	39.66497	35.705	54.66
2020	43.60934	30.119	46.94
2021	37.86769	33.413	63.94
2022	49.84933	61.525	37.11
2023	52.10321	38.091	57.37
2024	20.86538	25.500	54.61
2025	41.31501	47.266	54.76
2026	33.08702	36.387	43.58
2027	56.08242	51.171	34.66
2028	64.24603	37.642	46.91
2029	56.54352	39.311	36.12
2030	22.96999	47.543	62.53
2031	34.20818	27.236	38.94
2032	53.67458	44.221	40.46
2033	42.72022	49.044	30.89
2034	44.48209	50.753	61.28
2035	39.70259	44.216	45.55
2036	47.27356	41.163	31.28
2037	76.85988	51.525	43.96

2038	62.32694	35.653	30.67
2039	44.68479	55.899	33.42
2040	30.78315	47.668	34.24
2041	39.6506	33.138	36.26
2042	41.13341	44.204	37.19
2043	53.4278	43.447	42.24
2044	36.09163	45.177	38.98
2045	29.66711	57.015	67.19
2046	46.40982	60.701	27.25
2047	55.65701	35.222	76.35
2048	40.69816	44.762	55.70
2049	32.88202	37.870	47.44
2050	35.28659	42.718	57.42
2051	58.92524	45.856	37.17
2052	39.22736	50.030	23.40
2053	35.62452	36.009	45.83
2054	47.08407	45.170	43.28
2055	39.72457	35.343	68.28
2056	29.99022	65.162	31.88
2057	43.4929	30.265	27.26
2058	40.0485	32.709	28.19
2059	82.33642	58.606	29.83
2060	56.48761	82.828	55.47
2061	39.89108	48.574	87.36
2062	34.73032	49.215	45.34
2063	39.21705	27.270	41.92
2064	41.5507	93.814	48.55
2065	40.69927	43.739	40.05
2066	38.54787	62.448	37.81
2067	49.2338	30.695	43.22
2068	41.62116	36.980	57.70
2069	34.6986	45.649	56.08
2070	42.10195	72.245	37.55
2071	25.86632	37.988	55.51
2072	38.77699	48.252	43.66
2073	28.1056	44.555	58.32
2074	67.61863	48.759	28.67
2075	36.82727	59.058	46.06
2076	40.1619	41.898	58.50
2077	46.96967	29.850	35.47
2078	34.25636	39.844	35.05
2079	33.87169	41.633	61.95
2080	28.23784	57.564	72.76

2081	45.60183	47.244	58.74
2082	54.25554	37.537	72.05
2083	22.0559	40.981	44.21
2084	39.41858	34.337	61.29
2085	42.28307	47.888	29.63
2086	35.81371	57.430	40.09
2087	28.65652	66.901	58.96
2088	34.92259	37.336	42.13
2089	44.16422	46.244	64.23
2090	39.4304	39.608	25.54
2091	33.29272	30.975	36.00
2092	40.11237	34.809	65.06
2093	28.79	60.399	40.09
2094	47.08903	54.277	51.39
2095	26.71159	41.710	40.47
2096	37.41567	50.913	41.95
2097	48.71734	41.359	65.01
2098	36.83587	35.281	58.88
2099	64.10738	56.363	93.11
2100	48.30834	36.481	49.46

Appendix – E: Journal paper on Quantile Regression for selection of GCMs (Under Review)

Appendix – F: Journal paper on equidistance quantile matching method for updating IDF curves under climate change

Article Link: http://link.springer.com/article/10.1007%2Fs11269-014-0626-y

Appendix – G: List of Previous Reports in the Series
ISSN: (Print) 1913-3200; (online) 1913-3219
In addition to 53 previous reports (No. 01 – No. 53) prior to 2007

Predrag Prodanovic and Slobodan P. Simonovic (2007). Dynamic Feedback Coupling of Continuous Hydrologic and Socio-Economic Model Components of the Upper Thames River Basin. Water Resources Research Report no. 054, Facility for Intelligent Decision Support, Department of Civil and Environmental Engineering, London, Ontario, Canada, 437 pages. ISBN: (print) 978-0-7714-2638-4; (online) 978-0-7714-2639-1.

Subhankar Karmakar and Slobodan P. Simonovic (2007). Flood frequency analysis using copula with mixed marginal distributions. Water Resources Research Report no. 055, Facility for Intelligent Decision Support, Department of Civil and Environmental Engineering, London, Ontario, Canada, 144 pages. ISBN: (print) 978-0-7714-2658-2; (online) 978-0-7714-2659-9.

Jordan Black, Subhankar Karmakar and Slobodan P. Simonovic (2007). A web-based flood information system. Water Resources Research Report no. 056, Facility for Intelligent Decision Support, Department of Civil and Environmental Engineering, London, Ontario, Canada, 133 pages. ISBN: (print) 978-0-7714-2660-5; (online) 978-0-7714-2661-2.

Angela Peck, Subhankar Karmakar and Slobodan P. Simonovic (2007). Physical, economical, infrastructural and social flood risk - vulnerability analyses in GIS. Water Resources Research Report no. 057, Facility for Intelligent Decision Support, Department of Civil and Environmental Engineering, London, Ontario, Canada, 79 pages. ISBN: (print) 978-0-7714-2662-9; (online) 978-0-7714-2663-6.

Predrag Prodanovic and Slobodan P. Simonovic (2007). Development of rainfall intensity duration frequency curves for the City of London under the changing climate. Water Resources Research Report no. 058, Facility for Intelligent Decision Support, Department of Civil and Environmental Engineering, London, Ontario, Canada, 51 pages. ISBN: (print) 978-0-7714-2667-4; (online) 978-0-7714-2668-1.

Evan G. R. Davies and Slobodan P. Simonovic (2008). An integrated system dynamics model for analyzing behaviour of the social-economic-climatic system: Model description and model use guide. Water Resources Research Report no. 059, Facility for Intelligent Decision Support, Department of Civil and Environmental Engineering, London, Ontario, Canada, 233 pages. ISBN: (print) 978-0-7714-2679-7; (online) 978-0-7714-2680-3.

Vasan Arunachalam (2008). Optimization Using Differential Evolution. Water Resources Research Report no. 060, Facility for Intelligent Decision Support, Department of Civil and

Environmental Engineering, London, Ontario, Canada, 38 pages. ISBN: (print) 978-0-7714-2689-6; (online) 978-0-7714-2690-2.

Rajesh R. Shrestha and Slobodan P. Simonovic (2009). A Fuzzy Set Theory Based Methodology for Analysis of Uncertainties in Stage-Discharge Measurements and Rating Curve. Water Resources Research Report no. 061, Facility for Intelligent Decision Support, Department of Civil and Environmental Engineering, London, Ontario, Canada, 104 pages. ISBN: (print) 978-0-7714-2707-7; (online) 978-0-7714-2708-4.

Hyung-Il Eum, Vasan Arunachalam and Slobodan P. Simonovic (2009). Integrated Reservoir Management System for Adaptation to Climate Change Impacts in the Upper Thames River Basin. Water Resources Research Report no. 062, Facility for Intelligent Decision Support, Department of Civil and Environmental Engineering, London, Ontario, Canada, 81 pages. ISBN: (print) 978-0-7714-2710-7; (online) 978-0-7714-2711-4.

Evan G. R. Davies and Slobodan P. Simonovic (2009). Energy Sector for the Integrated System Dynamics Model for Analyzing Behaviour of the Social-Economic-Climatic Model. Water Resources Research Report no. 063, Facility for Intelligent Decision Support, Department of Civil and Environmental Engineering, London, Ontario, Canada, 191 pages. ISBN: (print) 978-0-7714-2712-1; (online) 978-0-7714-2713-8.

Leanna King, Tarana Solaiman and Slobodan P. Simonovic (2009). Assessment of Climatic Vulnerability in the Upper Thames River Basin. Water Resources Research Report no. 064, Facility for Intelligent Decision Support, Department of Civil and Environmental Engineering, London, Ontario, Canada, 62 pages. ISBN: (print) 978-0-7714-2816-6; (online) 978-0-7714-2817-3.

Slobodan P. Simonovic and Angela Peck (2009). Updated rainfall intensity duration frequency curves for the City of London under the changing climate. Water Resources Research Report no. 065, Facility for Intelligent Decision Support, Department of Civil and Environmental Engineering, London, Ontario, Canada, 64 pages. ISBN: (print) 978-0-7714-2819-7; (online) 978-0-7714-2820-3.

Leanna King, Tarana Solaiman and Slobodan P. Simonovic (2010). Assessment of Climatic Vulnerability in the Upper Thames River Basin: Part 2. Water Resources Research Report no. 066, Facility for Intelligent Decision Support, Department of Civil and Environmental Engineering, London, Ontario, Canada, 72 pages. ISBN: (print) 978-0-7714-2834-0; (online) 978-0-7714-2835-7.

Christopher J. Popovich, Slobodan P. Simonovic and Gordon A. McBean (2010). Use of an Integrated System Dynamics Model for Analyzing Behaviour of the Social-Economic-Climatic System in Policy Development. Water Resources Research Report no. 067, Facility for Intelligent Decision Support, Department of Civil and Environmental Engineering, London, Ontario, Canada, 37 pages. ISBN: (print) 978-0-7714-2838-8; (online) 978-0-7714-2839-5.

Hyung-Il Eum and Slobodan P. Simonovic (2009). City of London: Vulnerability of Infrastructure to Climate Change, Background Report #1 - Climate and Hydrologic Modeling. Water Resources Research Report no. 068, Facility for Intelligent Decision Support, Department of Civil and Environmental Engineering, London, Ontario, Canada, 103 pages. ISBN: (print) 978-0-7714-2844-9; (online) 978-0-7714-2845-6.

Dragan Sredojevic and Slobodan P. Simonovic (2009). City of London: Vulnerability of Infrastructure to Climate Change, Background Report #2 - Hydraulic Modeling and Floodplain Mapping. Water Resources Research Report no. 069, Facility for Intelligent Decision Support, Department of Civil and Environmental Engineering, London, Ontario, Canada, 147 pages. ISBN: (print) 978-0-7714-2846-3; (online) 978-0-7714-2847-0.

Tarana A. Solaiman and Slobodan P. Simonovic (2011). Quantifying Uncertainties in the Modelled Estimates of Extreme Precipitation Events at Upper Thames River Basin. Water Resources Research Report no. 070, Facility for Intelligent Decision Support, Department of Civil and Environmental Engineering, London, Ontario, Canada, 167 pages. ISBN: (print) 978-0-7714-2878-4; (online) 978-0-7714-2880-7.

Tarana A. Solaiman and Slobodan P. Simonovic (2011). Assessment of Global and Regional Reanalyses Data for Hydro-Climatic Impact Studies in the Upper Thames River Basin. Water Resources Research Report no. 071, Facility for Intelligent Decision Support, Department of Civil and Environmental Engineering, London, Ontario, Canada, 74 pages. ISBN: (print) 978-0-7714-2892-0; (online) 978-0-7714-2899-9.

Tarana A. Solaiman and Slobodan P. Simonovic (2011). Development of Probability Based Intensity-Duration-Frequency Curves under Climate Change. Water Resources Research Report no. 072, Facility for Intelligent Decision Support, Department of Civil and Environmental Engineering, London, Ontario, Canada, 89 pages. ISBN: (print) 978-0-7714-2893-7; (online) 978-0-7714-2900-2.

Dejan Vucetic and Slobodan P. Simonovic (2011). Water Resources Decision Making Under Uncertainty. Water Resources Research Report no. 073, Facility for Intelligent Decision Support, Department of Civil and Environmental Engineering, London, Ontario, Canada, 143 pages. ISBN: (print) 978-0-7714-2894-4; (online) 978-0-7714-2901-9.

Angela Peck, Elisabeth Bowering, and Slobodan P. Simonovic (2011). City of London: Vulnerability of Infrastructure to Climate Change, Final Report. Water Resources Research Report no. 074, Facility for Intelligent Decision Support, Department of Civil and Environmental Engineering, London, Ontario, Canada, 66 pages. ISBN: (print) 978-0-7714-2895-1; (online) 978-0-7714-2902-6.

M. Khaled Akhtar, Slobodan P. Simonovic, Jacob Wibe, Jim MacGee and Jim Davies (2011). An Integrated System Dynamics Model for Analyzing Behaviour of the Social-Energy-Economy-Climate System: Model Description. Water Resources Research Report no. 075, Facility for Intelligent Decision Support, Department of Civil and Environmental Engineering, London, Ontario, Canada, 211 pages. ISBN: (print) 978-0-7714-2896-8; (online) 978-0-7714-2903-3.

M. Khaled Akhtar, Slobodan P. Simonovic, Jacob Wibe, Jim MacGee and Jim Davies (2011). An Integrated System Dynamics Model for Analyzing Behaviour of the Social-Energy-Economy-Climate System: User's Manual. Water Resources Research Report no. 076, Facility for Intelligent Decision Support, Department of Civil and Environmental Engineering, London, Ontario, Canada, 161 pages. ISBN: (print) 978-0-7714-2897-5; (online) 978-0-7714-2904-0.

Nick Millington, Samiran Das and Slobodan P. Simonovic (2011). The Comparison of GEV, Log-Pearson Type 3 and Gumbel Distributions in the Upper Thames River Watershed under Global Climate Models. Water Resources Research Report no. 077, Facility for Intelligent Decision Support, Department of Civil and Environmental Engineering, London, Ontario, Canada, 53 pages. ISBN: (print) 978-0-7714-2898-2; (online) 978-0-7714-2905-7.

Andre Schardong and Slobodan P. Simonovic (2011). Multi-objective Evolutionary Algorithms for Water Resources Management. Water Resources Research Report no. 078, Facility for Intelligent Decision Support, Department of Civil and Environmental Engineering, London, Ontario, Canada, 167 pages. ISBN: (print) 978-0-7714-2907-1; (online) 978-0-7714-2908-8.

Samiran Das and Slobodan P. Simonovic (2012). Assessment of Uncertainty in Flood Flows under Climate Change. Water Resources Research Report no. 079, Facility for Intelligent Decision Support, Department of Civil and Environmental Engineering, London, Ontario, Canada, 67 pages. ISBN: (print) 978-0-7714-2960-6; (online) 978-0-7714-2961-3.

Rubaiya Sarwar, Sarah E. Irwin, Leanna King and Slobodan P. Simonovic (2012). Assessment of Climatic Vulnerability in the Upper Thames River basin: Downscaling with SDSM. Water Resources Research Report no. 080, Facility for Intelligent Decision Support, Department of Civil and Environmental Engineering, London, Ontario, Canada, 65 pages. ISBN: (print) 978-0-7714-2962-0; (online) 978-0-7714-2963-7.

Sarah E. Irwin, Rubaiya Sarwar, Leanna King and Slobodan P. Simonovic (2012). Assessment of Climatic Vulnerability in the Upper Thames River basin: Downscaling with LARS-WG. Water Resources Research Report no. 081, Facility for Intelligent Decision Support, Department of Civil and Environmental Engineering, London, Ontario, Canada, 80 pages. ISBN: (print) 978-0-7714-2964-4; (online) 978-0-7714-2965-1.

Samiran Das and Slobodan P. Simonovic (2012). Guidelines for Flood Frequency Estimation under Climate Change. Water Resources Research Report no. 082, Facility for Intelligent Decision Support, Department of Civil and Environmental Engineering, London, Ontario, Canada, 44 pages. ISBN: (print) 978-0-7714-2973-6; (online) 978-0-7714-2974-3.

Angela Peck and Slobodan P. Simonovic (2013). Coastal Cities at Risk (CCaR): Generic System Dynamics Simulation Models for Use with City Resilience Simulator. Water Resources Research Report no. 083, Facility for Intelligent Decision Support, Department of Civil and Environmental Engineering, London, Ontario, Canada, 55 pages. ISBN: (print) 978-0-7714-3024-4; (online) 978-0-7714-3025-1.

Abhishek Gaur and Slobodan P. Simonovic (2013). Climate Change Impact on Flood Hazard in the Grand River Basin, Ontario, Canada. Water Resources Research Report no. 084, Facility for Intelligent Decision Support, Department of Civil and Environmental Engineering, London, Ontario, Canada, 92 pages. ISBN: (print) 978-0-7714-3063-3; (online) 978-0-7714-3064-0.

Roshan Srivastav and Slobodan P. Simonovic (2014). Generic Framework for Computation of Spatial Dynamic Resilience. Water Resources Research Report no. 085, Facility for Intelligent Decision Support, Department of Civil and Environmental Engineering, London, Ontario, Canada, 81 pages. ISBN: (print) 978-0-7714-3067-1; (online) 978-0-7714-3068-8.

Angela Peck and Slobodan P. Simonovic (2014). Coupling System Dynamics with Geographic Information Systems: CCaR Project Report. Water Resources Research Report no. 086, Facility for Intelligent Decision Support, Department of Civil and Environmental Engineering, London, Ontario, Canada, 60 pages. ISBN: (print) 978-0-7714-3069-5; (online) 978-0-7714-3070-1.

Sarah Irwin, Roshan Srivastav and Slobodan P. Simonovic (2014). Instruction for Watershed Delineation in an ArcGIS Environment for Regionalization Studies. Water Resources Research Report no. 087, Facility for Intelligent Decision Support, Department of Civil and Environmental Engineering, London, Ontario, Canada, 45 pages. ISBN: (print) 978-0-7714-3071-8; (online) 978-0-7714-3072-5.

Andre Schardong, Roshan K. Srivastav and Slobodan P. Simonovic (2014).Computerized Tool for the Development of Intensity-Duration-Frequency Curves under a Changing Climate: Users Manual v.1.1. Water Resources Research Report no. 088, Facility for Intelligent Decision Support, Department of Civil and Environmental Engineering, London, Ontario, Canada, 68 pages. ISBN: (print) 978-0-7714-3085-5; (online) 978-0-7714-3086-2.